# Very High-Order Upwind Multi-Layer Compact (MLC) Schemes with Spectral-Like Resolution II: Two-Dimensional Case

Zeyu Bai[1] and Xiaolin Zhong[2]
*University of California, Los Angeles, CA, 90095, USA*

**In this paper, the very high-order upwind multi-layer compact (MLC) scheme developed by Bai and Zhong [1] is revisited and analyzed with focus on the two-dimensional case. The MLC scheme is designed to solve smooth multi-scale flow problems with complex physics, such as hypersonic boundary layer transition, turbulent flows, computational aeroacoustics, etc. In its multi-layer framework, the auxiliary equations for the first derivatives are introduced. Accordingly, the first derivatives are evolved simultaneously with the function values. The MLC scheme derived on structured grids has an explicit finite difference formulation, which includes both function values and first derivatives. Benefiting from the multi-layer framework, the scheme achieves very high-order accuracy and spectral-like resolution within a compact stencil. The upwind MLC scheme is derived on a centered stencil, with an adjustable parameter to introduce small dissipation for stability. A main problem of the original MLC scheme [1] is the minor numerical instability in the two-dimensional case, which is mainly triggered by the inconsistency between the 1-D and 2-D MLC formulations. Also, the approximation of the cross derivative in the original scheme introduces uncertainty, and it is relatively expensive in very high-order cases. In this paper, a directional discretization technique is designed to extend the 1-D MLC scheme to two-dimensional cases. By introducing the auxiliary equation for the cross derivative, the spatial discretization can be fulfilled along each dimension independently. Therefore, the 1-D MLC scheme can be applied to all spatial derivatives, and the 2-D MLC scheme is not required any more. This directional discretization technique avoids any inconsistency between the 1-D and 2-D MLC schemes, and it also overcomes the uncertainty arising from the approximation of cross derivatives. The Fourier analysis demonstrates that all modes of the new MLC scheme are stable in two-dimensional cases, and the new scheme has better spectral resolution and smaller anisotropic error for a large portion of wavenumbers in [0, $2\pi$]. The analysis through matrix method indicates that stable boundary closure schemes are also easier to be obtained for the new MLC scheme with the directional discretization. The numerical results validate that the new MLC scheme has smaller error and better computational efficiency than the original MLC scheme due to the better spectral resolution. The long-time simulation results verify that the original MLC scheme could be unstable in some cases; while the new MLC scheme with the directional discretization is always stable for both periodic and non-periodic boundary conditions.**

## I. Introduction

In the recent few decades, direct numerical simulation (DNS) has become one of the most important methods for the numerical study of various fluid dynamic problems with multiple scales and complex physics. Examples include the hypersonic boundary layer transition, turbulent flows, and computational aeroacoustics, etc. In [1], a brief description on these flow problems are given. A shared feature of them is the multiple scales embedded in the fields which are difficult to be captured with schemes of low-order accuracy. In the DNS investigation of multi-scale flow problems, the schemes should have very high-order of accuracy and high spectral resolution for a wide range of wavelength scales. The numerical dissipation and dispersion of such high-order schemes should be low enough to

[1] Graduate student researcher, Mechanical and Aerospace Engineering Department.
[2] Professor, Mechanical and Aerospace Engineering Department, AIAA associate fellow.

ensure that physical wave components with small amplitude are not suppressed or distorted, which is particularly important in computational aeroacoustics.

**High-Order Methods**

There are plenty of high-order numerical methods developed in the past few decades, such as spectral methods [2–4], compact finite difference schemes [5–12], discontinuous-Galerkin (DG) methods [13–16], and nonlinear schemes like TVD [17,18], ENO [19], WENO [20,21]. Many reviews are available for study on high-order methods. Ekaterinaris [22] presented a comprehensive review of the development of high-order methods with low numerical diffusion. Wang [23] discussed high-order methods with emphasize on unstructured grids. Shu [24] presented a detailed review of the development of high-order WENO schemes. A summary of popular high-order methods for smooth flow problems are also provided in [1].

Among these high-order methods, finite difference methods possess the advantages of simple formulations and high computational efficiencies; however, conventional explicit finite difference schemes face difficulty in resolving short waves, which limits their applications in multi-scale flow problems. To relax this constraint, finite difference schemes with spectral-like resolutions have been widely investigated. The compact scheme [5–12] is an influential alternative. Lele [5] performed extensive analysis on compact schemes and showed that through the implicit relation between the derivatives and function values on several grid points, the error in large wavenumber region is reduced and resolutions for short waves are improved. This idea has been extended by Chu & Fan [12,25] and Mahesh [10], by introducing the second derivatives in the implicit difference equation. The resulting scheme termed the combined compact difference (CCD) scheme, can achieve higher orders in accuracy and have better spectral resolution than the normal compact schemes on the same stencils. The dispersion-relation-preserving (DRP) scheme [26–30] is another widely used finite difference scheme with the spectral-like resolution. Tam and Webb [30] first proposed the DRP scheme by optimizing an explicit finite difference approximation in the wavenumber and frequency space, minimizing the $L_2$ norm error in modified wavenumbers, hence achieved spectral-like resolution. The general idea of these spectral-like finite difference schemes is to lower the error at marginal resolution related to high-frequency wave at the expense of allowing more error for low-frequency wave [31].

**Multi-Layer Compact Schemes**

Recently, the idea of using multiple degrees of freedom (DOFs) have been developed in quite a few numerical methods. The Discontinuous-Galerkin (DG) method is a typical example, where multiple DOFs determined by the order of accuracy is contained in each element. Orthogonal basis functions are usually utilized to construct the high-order piecewise polynomials within the element, and all the weights of the basis are solved as unknowns. Spectral difference (SD) methods [32–34] and spectral volume (SV) methods [35–38] also contain multiple DOFs in each element, they are similar to DG methods but the way the piecewise polynomials are constructed is different. SV methods define the sub-cells, and the averaged conservative variables in each sub-cell are DOFs; while SD methods define the solution points within each element, and point values are DOFs [23]. These point or sub-cell values are then used to construct polynomials. DG methods and other finite element methods usually possess high-order accuracy and can be easily applied to flow simulations over complex geometries with unstructured grids, and they are extremely compact because the high-order polynomials are defined at each cell, and no reconstructions are required. However, they require plenty of memories, especially in multi-dimensional simulations. The idea of evolving multiple degrees of freedom (DOFs) has also appeared in finite volume or finite difference methods. Qiu and Shu, et al. developed a fifth-order Hermite WENO (HWENO) scheme [39–41] in the finite volume framework, where both function value and its first derivative is solved and used in the reconstruction. Balsara et al. [42] also used HWENO approach in their hybrid RKDG+HWENO schemes, where a monotonicity preserving strategy that is scale-free and problem-independent for detecting troubled zones is proposed. They proved that they are good alternatives with lower storage and narrower stencils to Runge-Kutta Discontinuous Galerkin (RKDG) schemes. Luo et al. [43–45] did extensive work on the HWENO schemes with a focus on unstructured grids. They applied HWENO approach as limiters to both original discontinuous-Galerkin (DG) methods and reconstructed DG methods and found that it can save computational cost, enhance accuracy, and ensure linear stability. The major advantage of these HWENO approaches is the compactness of stencils for reconstructions, consequently, they are very suitable as limiters for discontinuous-Galerkin methods. Some compact finite difference schemes [46–48] introduce half grid points and save the independent variables on these grid points for spatial discretization, which can also be regarded as a method with multiple DOFs. In general, the numerical schemes with multiple DOFs attain benefits from their compact support stencil, leading to better efficiency for parallel computing and simpler stable boundary conditions. Most of the methods mentioned above utilized this desirable feature to improve their performance.

To improve the performance of finite difference methods on smooth multi-scale flow problems with complex physics, the authors developed a new very high-order upwind multi-layer compact (MLC) scheme [1]. It has the properties of simple formulation, compact stencil, low dissipation, high-order accuracy, and spectral-like resolution.

In the MLC scheme, the auxiliary equations for the first derivatives are introduced, thus the first derivatives are saved as the additional degrees of freedom (DOFs), and evolved simultaneously with the function values. Both function values and first derivatives are used for approximation of higher derivatives. Benefiting from the multi-layer framework, the scheme achieves very high-order accuracy and spectral-like resolution within a compact stencil. The upwind MLC scheme is derived on a centered stencil, with an adjustable parameter to introduce small dissipation for stability. Fourier analysis shows that the MLC schemes have small dissipation and dispersion in a very wide range of wavenumbers in both one- and two-dimensional cases; and the anisotropic error is much smaller than conventional finite difference methods in the two-dimensional case. The numerical results demonstrate that good computational efficiency, very high-order of accuracies, and superior resolutions on coarse meshes can be achieved by the MLC schemes.

However, the MLC scheme developed in [1] still have some remaining problems to be addressed for two-dimensional simulations. In the first place, the two-dimensional Fourier analysis shows that a minor numerical instability appears in a very narrow range of wavenumbers. The instability is mainly triggered by the inconsistency between 1-D and 2-D MLC formulations. For example, the 1-D upwind scheme is used for the second derivative, while the 2-D central scheme is used for the cross derivative in the MLC scheme. Although the amplification factor related to the minor numerical instability is very small, it may still lead to potential risk in two-dimensional flow simulations. In the second place, the approximation of the cross derivative uses the square stencil where redundant information exists. Therefore, the formula for cross-derivative approximation is not unique and supporting points need to be selected manually. There exist difficulties in two aspects: it is hard to determine the appropriate supporting points and find the optimal formula; and it is hard to derive the 2-D upwind scheme that is compatible with the 1-D upwind scheme, which in turn causes the first problem of inconsistency. This uncertainty of the MLC scheme may also affect the accuracy and the stability of the MLC scheme. In the third place, the cross-derivative approximation on the square stencil is relatively expensive compared with the second-derivative approximation. In the cases of very high-order schemes, it becomes a negligible factor which limits the improvement of the computational efficiency.

To overcome the minor numerical instability, remove the uncertainty, and improve the accuracy and the computational efficiency, a directional discretization technique is designed in this paper. Then, the 1-D MLC scheme can be extended to two-dimensional cases naturally. Similar idea can be found in the central Hermite WENO scheme developed by Tao et al [49], though their method is based on the finite volume framework. In their methods, the equation of the mixed first-order momentum is introduced when the dimension is higher than one. All zeroth-order and first-order moments, which are integral quantities in each cell, are used in the spatial reconstruction through a dimension-by-dimension strategy. In our directional discretization technique, only values and spatial derivatives at discrete grid points are used for simpler implementation. The auxiliary equation for the cross derivative is introduced in the two-dimensional case; then, the spatial discretization of the entire system can be fulfilled along each dimension independently. Therefore, the 1-D MLC scheme can be naturally extended to two-dimensional cases, and no formula of the 2-D MLC scheme is required. With this directional discretization technique, any inconsistency between the 1-D and 2-D MLC scheme can be avoided, and the uncertainty arising from the approximation of cross derivatives is overcome. In the following part of this paper, the numerical method developed in [1] is termed as the original MLC scheme, and the new numerical method presented in this paper is termed as the new MLC scheme.

The context of the paper is organized as follows. In Chapter II, the formulation of the original MLC scheme is revisited, and the new MLC scheme is illustrated on the two-dimensional linear advection equation. In Chapter III, the Fourier analysis and boundary stability analysis with the matrix method are carried out to show the dissipative and dispersive errors, the spectral resolution, the anisotropy, and the stability of the new MLC scheme in two-dimensional cases. In Chapter IV, the new MLC scheme is assessed on the linear advection equation with both periodic and non-periodic boundary conditions, and the nonlinear Euler equations using the 2-D entropy wave and 2-D isentropic vortex as test cases. In Chapter 5, the summary and main conclusions of this paper are given.

## II. Very High-Order Upwind Multi-Layer Compact (MLC) Schemes

Fluid dynamic problems are governed by the Navier-Stokes equations. In the inviscid flow, the viscous term can be eliminated, and the resulting governing equations become the nonlinear Euler equation, which can be written in the following conservation-law form in the Cartesian coordinate,

$$\frac{\partial U}{\partial t}+\frac{\partial F_j}{\partial x_j}=0 \tag{1}$$

where $U$ and $F_j$ are the vectors of conservative variables and inviscid convective flux in the direction of $x_j$ respectively,

$$U = \left[\rho,\ \rho u_1,\ \rho u_2,\ \rho u_3,\ E_t\right]^T \tag{2}$$

$$F_j = \begin{bmatrix} \rho u_j \\ \rho u_1 u_j + p\delta_{1j} \\ \rho u_2 u_j + p\delta_{2j} \\ \rho u_3 u_j + p\delta_{3j} \\ \left(E_t + p\right)u_j \end{bmatrix} \tag{3}$$

In a wide range of temperature and pressure, the perfect gas assumption can be used, and the total energy per unit volume $E_t$ is calculated from,

$$E_t = \frac{p}{\gamma - 1} + \frac{1}{2}\rho u_k u_k \tag{4}$$

The method of lines can be used to discretize the governing equations by separating spatial and temporal discretization. The main difficulty in the spatial discretization is the approximation of the hyperbolic-type convective term in Eq. (1), which plays an important role in numerical stability. The very high-order upwind MLC scheme derived in [1] can be utilized to discretize the convective term.

In the following part of this section, the linear advection equation, which is the model equation of the Euler equations, is used to illustrate the implementation of the original MLC scheme and the new MLC scheme with directional discretization.

**A. Original MLC Schemes for Two-Dimensional Cases**

The derivation of the original MLC scheme is briefly reviewed in this section, and more details can be found in [1]. The two-dimensional advection equation in the Cartesian coordinate is used to illustrate the derivation in the two-dimensional case,

$$\frac{\partial u}{\partial t} + c_1 u_x + c_2 u_y = 0 \tag{5}$$

where $u$ is a scalar, and $c_1$, $c_2$ are advection speeds in $x$ and $y$ directions respectively. Taking the gradient on Eq. (5), a system of partial differential equations are derived in the following form,

$$\frac{\partial}{\partial t}\begin{bmatrix} u \\ v \\ w \end{bmatrix} = -c_1\begin{bmatrix} v \\ u_{xx} \\ u_{xy} \end{bmatrix} - c_2\begin{bmatrix} w \\ u_{xy} \\ u_{yy} \end{bmatrix} \tag{6}$$

where $u$, $v$ ($=u_x$), $w$ ($=u_y$) are unknowns. The original equation needs no approximation because $v$ and $w$ are part of the solution, as Eq. (6) shows. The spatial discretization only applies to the last two equations in (6).

The computational domain for two-dimensional advection is a square within the range of $a \le x \le b$ and $a \le y \le b$, where four boundaries can be either periodic or non-periodic. A uniform mesh is used for the computational domain with the grid spacing $h$ in both dimensions. To discretize the system, $u_{xx}$ and $u_{yy}$ in Eq. (6) are approximated using the 1-D upwind MLC scheme along $x$ and $y$ directions, and $u_{xy}$ is approximated using the 2-D central MLC scheme which is one-order higher than the 1-D upwind scheme in accuracy. There are three degrees of freedom (DOFs) - $u_{i,j}$, $v_{i,j}$, and $w_{i,j}$ at the grid point $(i, j)$. Fig. 1 shows the stencil of the $L_1$-$L_2$-$M_1$-$M_2$ MLC scheme for two-dimensional cases, where $(i, j)$ is the base point. Only the information at the center line along $x$ or $y$ axis is used to approximate $(u_{xx})_{i,j}$ or $(u_{yy})_{i,j}$ respectively, while all points in the square can be considered for the approximation of $(u_{xy})_{i,j}$.

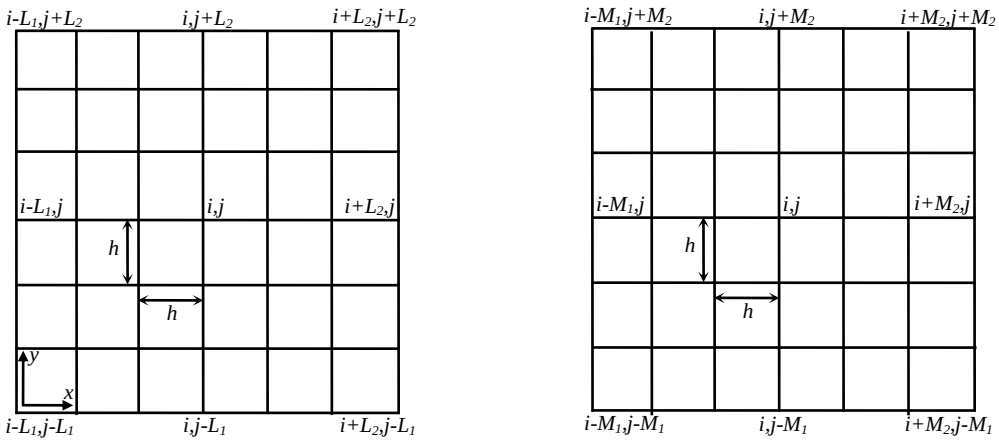


a), function value layer b), first derivative layers

**Fig. 1. Stencil of the $L_1$-$L_2$-$M_1$-$M_2$ MLC scheme for two-dimensional cases.**

Using the 1-D upwind MLC scheme with the $L_1$-$L_2$-$M_1$-$M_2$ stencil, $(u_{xx})_{i,j}$ and $(u_{yy})_{i,j}$ can be approximated as,

$$\left(u_{xx}\right)_{i,j} = \frac{1}{h^2}\sum_{l=-L_1}^{L_2} a_l u_{i+l,j} + \frac{1}{h}\sum_{m=-M_1}^{M_2} b_m v_{i+m,j} - \frac{\alpha}{(p+2)!}\left(\frac{\partial u}{\partial x^{p+2}}\right)_{i,j} h^p + o\left(h^{p+1}\right) \tag{7}$$

$$\left(u_{yy}\right)_{i,j} = \frac{1}{h^2}\sum_{l=-L_1}^{L_2} a_l u_{i,j+l} + \frac{1}{h}\sum_{m=-M_1}^{M_2} b_m w_{i,j+m} - \frac{\alpha}{(p+2)!}\left(\frac{\partial u}{\partial y^{p+2}}\right)_{i,j} h^p + o\left(h^{p+1}\right) \tag{8}$$

$$p = L_1 + L_2 + M_1 + M_2 - 1 \tag{9}$$

where coefficients $a_l$ and $b_m$ can be derived from the Taylor series expansion. In the truncation error term, $\alpha$ is an adjustable parameter. Non-zero $\alpha$'s lead to upwind or downwind schemes, which have a $p$-th order of accuracy. When $\alpha = 0$, the central scheme with the maximum ($p$+1)-th order is obtained. The value of $\alpha$ has an impact on the stability, accuracy, and stiffness of the MLC scheme. Larger $\alpha$ leads to better stability, larger dissipation and stiffness, and it slightly increases dispersion. Therefore, the value of $\alpha$ needs to be large enough to make the scheme stable and needs to be relatively small to control the dissipation and dispersion. In Eqs. (7) and (8), the same MLC scheme is applied to $x$ and $y$ dimensions respectively.

Similarly, the cross derivative $(u_{xy})_{i,j}$ can be approximated using the corresponding 2-D central MLC scheme as follows,

$$\left(u_{xy}\right)_{i,j} = \frac{1}{h^2}\sum_{\substack{l_x=-L_1\\ l_y=-L_1}}^{L_2} a_{l_x,l_y} u_{i+l_x,j+l_y} + \frac{1}{h}\sum_{\substack{m_x=-M_1\\ m_y=-M_1}}^{M_2} b_{m_x,m_y} v_{i+m_x,j+m_y} + \frac{1}{h}\sum_{\substack{n_x=-M_1\\ n_y=-M_1}}^{M_2} c_{n_x,n_y} w_{i+n_x,j+n_y} + o\left(h^{p+1}\right) \tag{10}$$

which has a ($p$+1)-th order of accuracy without an upwind truncation error term. The coefficients $a$, $b$, $c$ in Eq. (10) can be derived by multivariate Taylor series expansion. In the stencil for cross derivatives, the layer for function values contains $(L_1+L_2+1)^2$ gird points, and each layer for first derivatives contains $(M_1+M_2+1)^2$ gird points. It can be proven that the linear system of equations with all the points is underdetermined due to redundant information. To get a unique solution of $a$, $b$, $c$'s, we must preselect the supporting points in both value and derivative layers. In Eq. (10), only the coefficients for preselected terms are treated as unknowns, and the coefficients for other terms are set to be zero. The criterion is to find the simplest formula which contains the fewest non-zero terms with relatively concise coefficients, which can reduce both the computational cost and the round-off error. Because the 2-D central schemes are one order higher than the 1-D upwind schemes, their combination can maintain at least an overall accuracy of $p$-th order.

Several typical 1-D and 2-D MLC schemes are presented in the following part of this section. For the 1-D upwind scheme, the recommended $\alpha$ values are selected based on one-dimensional Fourier analysis results. More details can be found in [1]. In two-dimensional simulations, ($u'$, $u''$) in the following 1-D formulas are simply replaced by ($v$, $u_{xx}$) or ($w$, $u_{yy}$), as in Eqs. (7) and (8).

***One-Dimensional 1-1-1-1 Scheme (3rd Order)***

Using a three-point stencil in both value and first derivative layers as shown in Fig. 2, the coefficients $a_l$ and $b_m$ in Eqs. (7) or (8) can be solved as,

$$
\begin{aligned}
&a_{\pm1} = 2 \mp \frac{3}{4}\alpha, \qquad a_0 = -4, \\
&b_{\pm1} = \mp\frac{1}{2} + \frac{1}{4}\alpha, \qquad b_0 = \alpha.
\end{aligned}
\tag{11}
$$

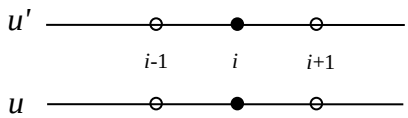


**Fig. 2. Stencil of the 1-1-1-1 scheme (3rd order) for second derivative approximations.**

The recommended value of $\alpha$ is 1.5 based on the Fourier analysis, and the formula for the third-order 1-1-1-1 scheme can be obtained,

$$
u_i'' = \frac{1}{h^2}\left(\frac{25}{8}u_{i-1} - 4u_i + \frac{7}{8}u_{i+1}\right) + \frac{1}{h}\left(\frac{7}{8}u_{i-1}' + \frac{3}{2}u_i' - \frac{1}{8}u_{i+1}'\right) \tag{12}
$$

***One-Dimensional 2-2-1-1 Scheme (5th Order)***

Using a five-point stencil for values and a three-point stencil for first derivatives as shown in Fig. 3, the coefficients $a_l$ and $b_m$ in Eqs. (7) or (8) can be solved as,

$$
\begin{aligned}
&a_{\pm2} = \frac{1}{36} \pm \frac{1}{144}\alpha, \qquad a_{\pm1} = \frac{20}{9} \pm \frac{7}{36}\alpha, \qquad a_0 = -\frac{9}{2}, \\
&b_{\pm1} = \mp\frac{2}{3} - \frac{1}{12}\alpha, \qquad b_0 = -\frac{1}{4}\alpha.
\end{aligned}
\tag{13}
$$

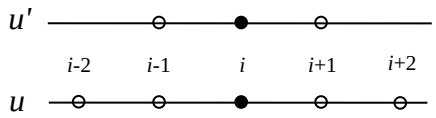


**Fig. 3. Stencil of the 2-2-1-1 scheme (5th order) for second derivative approximations.**

The recommended value of $\alpha$ is -1 based on the Fourier analysis, and the formula for the fifth-order 2-2-1-1 scheme can be obtained,

$$
u_i'' = \frac{1}{h^2}\left(\frac{5}{144}u_{i-2} + \frac{29}{12}u_{i-1} - \frac{9}{2}u_i + \frac{73}{36}u_{i+1} + \frac{1}{48}u_{i+2}\right) + \frac{1}{h}\left(\frac{3}{4}u_{i-1}' + \frac{1}{4}u_i' - \frac{7}{12}u_{i+1}'\right) \tag{14}
$$

***One-Dimensional 2-2-2-2 Scheme (7th Order)***

Using a five-point stencil in both value and first derivative layers as shown in Fig. 4, the coefficients $a_l$ and $b_m$ in Eqs. (7) or (8) can be solved as,

$$
\begin{aligned}
&a_{\pm2} = \frac{7}{54} \mp \frac{25}{3456}\alpha, \qquad a_{\pm1} = \frac{64}{27} \mp \frac{5}{108}\alpha, \qquad a_0 = -5, \\
&b_{\pm2} = \mp\frac{1}{36} + \frac{1}{576}\alpha, \qquad b_{\pm1} = \mp\frac{8}{9} + \frac{1}{36}\alpha, \qquad b_0 = \frac{1}{16}\alpha.
\end{aligned}
\tag{15}
$$

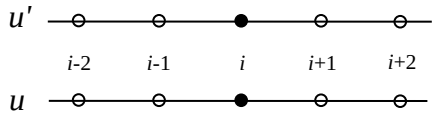


**Fig. 4. Stencil of the 2-2-2-2 scheme (7th order) for second derivative approximations.**

The recommended value of $\alpha$ is 12 based on the Fourier analysis, and the formula for the seventh-order 2-2-2-2 scheme can be obtained,

$$u_i'' = \frac{1}{h^2}\left(\frac{187}{864}u_{i-2} + \frac{79}{27}u_{i-1} - 5u_i + \frac{49}{27}u_{i+1} + \frac{37}{864}u_{i+2}\right) + \frac{1}{h}\left(\frac{7}{144}u'_{i-2} + \frac{11}{9}u'_{i-1} + \frac{3}{4}u'_i - \frac{5}{9}u'_{i+1} - \frac{1}{144}u'_{i+2}\right) \tag{16}$$

***Two-Dimensional 1-1-1-1 Scheme (4th Order)***

The stencil to approximate $u_{xy}$ in the two-dimensional fourth-order 1-1-1-1 scheme is shown in Fig. 5, where the preselected supporting points for values and first derivatives are marked with black dots. Following the criterion of keeping fewest non-zero terms with relatively concise coefficients in Eq. (10), a specific formula for the two-dimensional fourth-order 1-1-1-1 scheme is derived as follows,

$$\left(u_{xy}\right)_{i,j} = \frac{1}{h^2}\left(-\frac{1}{4}u_{i-1,j-1} + \frac{1}{4}u_{i+1,j-1} + \frac{1}{4}u_{i-1,j+1} - \frac{1}{4}u_{i+1,j+1}\right) + \frac{1}{h}\left(-\frac{1}{2}\left(u_x\right)_{i,j-1} + \frac{1}{2}\left(u_x\right)_{i,j+1}\right) + \frac{1}{h}\left(-\frac{1}{2}\left(u_y\right)_{i-1,j} + \frac{1}{2}\left(u_y\right)_{i+1,j}\right) \tag{17}$$

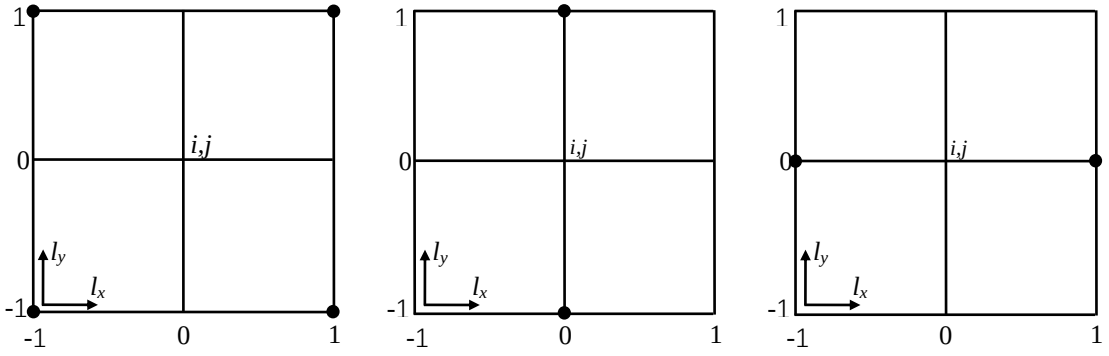


a), $u$ b), $u_x$ c), $u_y$

**Fig. 5. Stencil and supporting points of the 1-1-1-1 scheme (4th order) for cross-derivative approximations.**

In total, four value points, two $x$ derivative points, and two $y$ derivative points are preselected. The locations and coefficients of supporting points are symmetric, which is the indication of central schemes. It turns out other formulas can also achieve the same order of accuracy, but they are more complicated than Eq. (17).

***Two-Dimensional 2-2-1-1 Scheme (6th Order)***

The stencil to approximate $u_{xy}$ in the two-dimensional sixth-order 2-2-1-1 scheme is shown in Fig. 6. Following the same criterion as in the 1-1-1-1 scheme, a specific formula for the two-dimensional sixth-order 2-2-1-1 scheme is derived as follows,

$$\begin{aligned}\left(u_{xy}\right)_{i,j} = {} & \frac{1}{h^2}\left(\frac{1}{144}u_{i-2,j-2} - \frac{1}{144}u_{i+2,j-2} + \frac{5}{9}u_{i-1,j-1} - \frac{5}{9}u_{i+1,j-1} - \frac{5}{9}u_{i-1,j+1} + \frac{5}{9}u_{i+1,j+1} - \frac{1}{144}u_{i-2,j+2} + \frac{1}{144}u_{i+2,j+2}\right) \\ & + \frac{1}{h}\left(\frac{1}{6}\left(u_x\right)_{i-1,j-1} + \frac{1}{6}\left(u_x\right)_{i+1,j-1} - \frac{1}{6}\left(u_x\right)_{i-1,j+1} - \frac{1}{6}\left(u_x\right)_{i+1,j+1}\right) \\ & + \frac{1}{h}\left(\frac{1}{6}\left(u_y\right)_{i-1,j-1} - \frac{1}{6}\left(u_y\right)_{i+1,j-1} + \frac{1}{6}\left(u_y\right)_{i-1,j+1} - \frac{1}{6}\left(u_y\right)_{i+1,j+1}\right)\end{aligned} \tag{18}$$

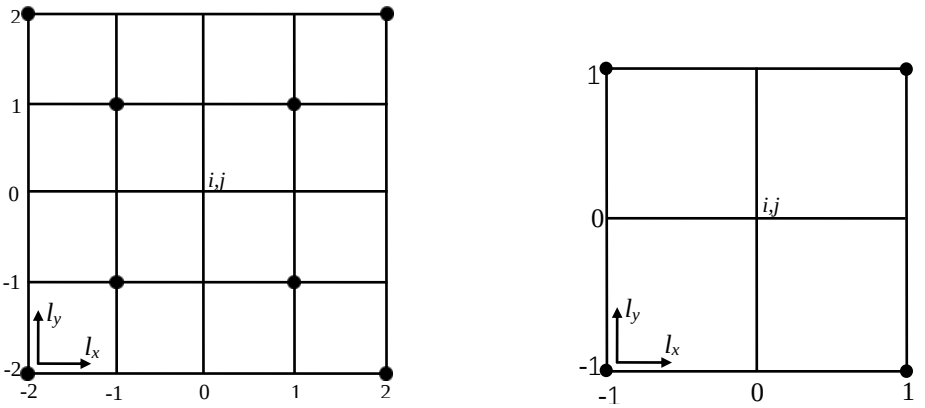


a), $u$ b), $u_x$ and $u_y$

**Fig. 6. Stencil and supporting points of the 2-2-1-1 scheme (6th order) for cross-derivative approximations.**

In total, eight value points, four $x$ derivative points, and four $y$ derivative points are preselected. Again, many other formulas which are more complicated than Eq. (18) may achieve the same order of accuracy.

***Two-Dimensional 2-2-2-2 Scheme (8th Order)***

The stencil to approximate $u_{xy}$ in the two-dimensional eighth-order 2-2-2-2 scheme is shown in Fig. 7. Following the same criterion as in the 1-1-1-1 and 2-2-1-1 schemes, a specific formula for the two-dimensional eighth-order 2-2-2-2 scheme is derived as follows,

$$\begin{aligned}\left(u_{xy}\right)_{i,j} = \frac{1}{h^2}\Bigg(&-\frac{1}{144}u_{i-2,j-2}+\frac{1}{18}u_{i-1,j-2}-\frac{1}{18}u_{i+1,j-2}+\frac{1}{144}u_{i+2,j-2}+\frac{1}{18}u_{i-2,j-1}-\frac{4}{9}u_{i-1,j-1}+\frac{4}{9}u_{i+1,j-1}-\frac{1}{18}u_{i+2,j-1}\\ &-\frac{1}{18}u_{i-2,j+1}+\frac{4}{9}u_{i-1,j+1}-\frac{4}{9}u_{i+1,j+1}+\frac{1}{18}u_{i+2,j+1}+\frac{1}{144}u_{i-2,j+2}-\frac{1}{18}u_{i-1,j+2}+\frac{1}{18}u_{i+1,j+2}-\frac{1}{144}u_{i+2,j+2}\Bigg)\\ &+\frac{1}{h}\left(\frac{1}{12}\left(u_x\right)_{i,j-2}-\frac{2}{3}\left(u_x\right)_{i,j-1}+\frac{2}{3}\left(u_x\right)_{i,j+1}-\frac{1}{12}\left(u_x\right)_{i,j+2}\right)\\ &+\frac{1}{h}\left(\frac{1}{12}\left(u_y\right)_{i-2,j}-\frac{2}{3}\left(u_y\right)_{i-1,j}+\frac{2}{3}\left(u_y\right)_{i+1,j}-\frac{1}{12}\left(u_y\right)_{i+2,j}\right)\end{aligned} \tag{19}$$

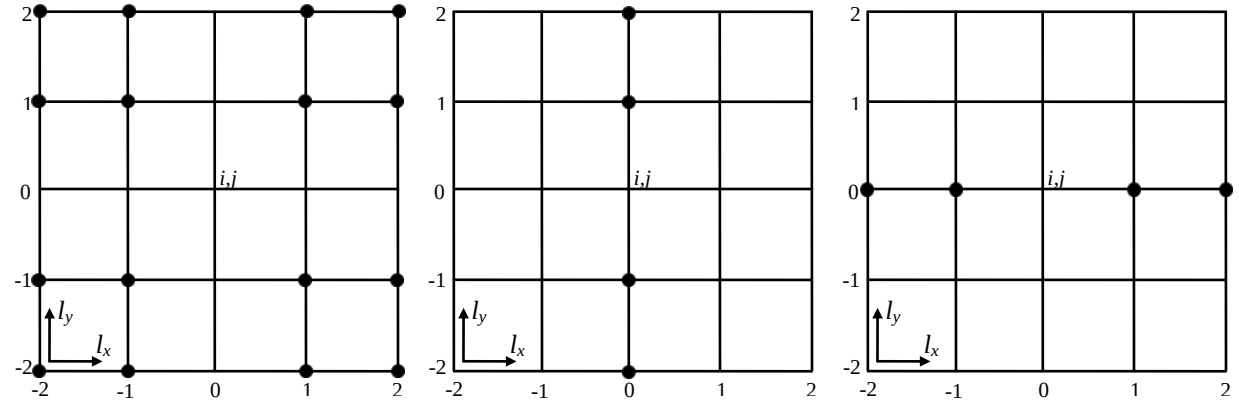


a), $u$ b), $u_x$ c), $u_y$

**Fig. 7. Stencil and supporting points of the 2-2-2-2 scheme (8th order) for cross-derivative approximations.**

In total, sixteen value points, four $x$ derivative points, and four $y$ derivative points are preselected. This specific 2-2-2-2 scheme has the simplest formula among all 2-2-2-2 schemes with the eighth-order of accuracy.

**B. New MLC Schemes with Directional Discretization for Two-Dimensional Cases**

There is a remaining problem in the original MLC schemes presented in Section II.A, which is the minor numerical instability indicated by the two-dimensional Fourier analysis. The analysis results are presented in next chapter. There are two possible reasons behind the minor instability. First, the formula for the 2-D MLC schemes

used for cross-derivative approximations are not unique because of the redundant information within the square stencil, as shown in Fig. 1. Although the criterion of keeping fewest non-zero terms with relatively concise coefficients in the formula is reasonable for the selection of the supporting points, it mainly focuses on improving the computational efficiency and reducing the round-off error. It is unpractical to conduct rigorous mathematical analysis or numerical tests to compare the performance such as stability, dissipation, dispersion, and anisotropy among numerous candidates. Therefore, the uncertainty always exists in the derivation of the 2-D MLC schemes. Second, it is difficult to generalize the idea of constructing upwind schemes on centered stencils to the 2-D MLC schemes. As shown in the one-dimensional $L_1$-$L_2$-$M_1$-$M_2$ scheme in Eqs. (7) or (8), one of the novelty of the MLC scheme is using an adjustable parameter $\alpha$ to introduce small numerical dissipation for stability, and to make a central scheme "upwind". However, there are multiple leading truncation error terms with the same degree – $h^p$ in Eq. (10) when it is expanded at the base point $(i, j)$ through the multivariate Taylor series as follows,

$$\begin{aligned}\left(u_{xy}\right)_{i,j} = &\frac{1}{h^2}\sum_{\substack{l_x=-L_1\\ l_y=-L_1}}^{L_2} a_{l_x,l_y} u_{i+l_x,j+l_y} + \frac{1}{h}\sum_{\substack{m_x=-M_1\\ m_y=-M_1}}^{M_2} b_{m_x,m_y} v_{i+m_x,j+m_y} + \frac{1}{h}\sum_{\substack{n_x=-M_1\\ n_y=-M_1}}^{M_2} c_{n_x,n_y} w_{i+n_x,j+n_y} \\ &+ \sum_{k=0}^{p+2} \alpha_k \left(\frac{\partial u}{\partial x^k \partial y^{p+2-k}}\right)_{i,j} h^p + o\left(h^{p+1}\right)\end{aligned} \tag{20}$$

Specifically, a 2-D upwind scheme with $p$-th order of accuracy contains a total of ($p$+3) leading truncation error terms. How to choose the coefficients $\alpha_k$ of all truncation error terms is unclear and complicated. On the other hand, the upwind schemes possess more uncertainty than the central schemes because the supporting points can be distributed asymmetrically, which makes the preselection of points more complicated. Considering all the complexity, the 2-D central schemes are used in the original MLC schemes for two-dimensional cases. However, it may not be consistent with the 1-D upwind schemes.

The remaining problems in the original MLC scheme are all related to the approximation of cross derivatives for two-dimensional cases. It gives us the motivation to seek a numerical method which can avoid the approximation of cross derivatives. Therefore, a directional discretization technique is designed in this paper. The following discussion is continued with the two-dimensional advection equations (6). The cross derivative $u_{xy}$ is treated as another unknown, and its auxiliary equation is introduced by taking derivatives of Eq. (5) in both $x$ and $y$ directions as follows,

$$\frac{\partial u_{xy}}{\partial t} + c_1 u_{xxy} + c_2 u_{xyy} = 0 \tag{21}$$

In Eq. (21), higher derivatives $u_{xxy}$ and $u_{xyy}$ appears which seems to make the spatial discretization more complicated. However, both the first derivative $u_x$, $u_y$ and cross derivative $u_{xy}$ are solved as the unknowns and saved at each grid point. These discrete derivatives can be used to approximate higher derivatives through the MLC schemes. In other words, $u_{xxy}$ can be approximated from $u_y$ and $u_{xy}$, and $u_{xyy}$ can be approximated from $u_x$ and $u_{xy}$. It is obvious that these approximations can be performed along each dimension $x$ or $y$ independently. Therefore, only the 1-D MLC schemes described in section II.A is needed for the spatial discretization. Adding the new auxiliary equation (21) into Eq. (6) and introducing the notation $r = u_{xy}$, a new system of partial differential equations for the new MLC scheme can be derived as,

$$\frac{\partial}{\partial t}\begin{bmatrix} u \\ v \\ w \\ r \end{bmatrix} = -c_1 \begin{bmatrix} v \\ u_{xx} \\ r \\ w_{xx} \end{bmatrix} - c_2 \begin{bmatrix} w \\ r \\ u_{yy} \\ v_{yy} \end{bmatrix} \tag{22}$$

where $u$, $v$, $w$, and $r$ are treated as unknows.

There are four degrees of freedom at each grid point in the new MLC scheme for two-dimensional case, which slightly increases the memory requirement compared with three degrees of freedom in the original MLC scheme. However, the benefit of the additional unknown $r$ is significant.

First, only approximations for second derivatives $u_{xx}$, $w_{xx}$, $u_{yy}$, $v_{yy}$ are needed in Eq. (22). In other words, the uncertainty in the approximation of $u_{xy}$ is avoided.

Second, the discretization can be carried out along each grid line with the following formulas,

$$\begin{pmatrix} u_{xx} \\ w_{xx} \end{pmatrix}_{i,j} = \frac{1}{h^2}\sum_{l=-L_1}^{L_2} a_l \begin{pmatrix} u \\ w \end{pmatrix}_{i+l,j} + \frac{1}{h}\sum_{m=-M_1}^{M_2} b_m \begin{pmatrix} v \\ r \end{pmatrix}_{i+m,j} - \frac{\alpha}{(p+2)!}\left(\partial \begin{pmatrix} u \\ w \end{pmatrix} \Big/ \partial x^{p+2}\right)_{i,j} h^p + \cdots \tag{23}$$

$$\begin{pmatrix} u_{yy} \\ v_{yy} \end{pmatrix}_{i,j} = \frac{1}{h^2}\sum_{l=-L_1}^{L_2} a_l \begin{pmatrix} u \\ v \end{pmatrix}_{i,j+l} + \frac{1}{h}\sum_{m=-M_1}^{M_2} b_m \begin{pmatrix} w \\ r \end{pmatrix}_{i,j+m} - \frac{\alpha}{(p+2)!}\left(\partial \begin{pmatrix} u \\ v \end{pmatrix} \Big/ \partial y^{p+2}\right)_{i,j} h^p + \cdots \tag{24}$$

where $p$ is the order of accuracy, and $\alpha$ is the upwind coefficient. It is obvious the same 1-D MLC scheme as in Eqs. (7) and (8) can be applied to $u_{xx}$, $w_{xx}$, $u_{yy}$, $v_{yy}$, therefore, the spatial discretization becomes rigorously consistent for one- or two-dimensional cases. All the properties of 1-D scheme can be naturally generalized to the two-dimensional case, and the implementation of the upwind scheme ($\alpha \neq 0$) is straightforward as well.

Third, the spatial discretization becomes more computational efficient with the directional discretization technique. As we can see in Eqs. (6) and (22), although the new MLC scheme introduces an additional equation to solve, there are still four spatial derivative terms to deal with which is the same as the original MLC scheme. Note that for the original scheme, the same cross derivative $u_{xy}$ appears twice in Eq. (6); however, this is just a special case for the linear advection equation. In nonlinear equations like the Euler and Navier-Stokes equations, there will be two different cross derivatives to approximate. The 2-D approximation for $u_{xy}$ is more expensive compared with the 1-D approximations for $u_{xx}$, $w_{xx}$, $u_{yy}$, $v_{yy}$. If the stencil has $n$ points, the CPU time to approximate a cross derivative is $o(n^2)$, while it only takes $o(n)$ CPU time in a second derivative approximation. In very high-order cases where wider stencils are required, the CPU time for cross-derivative approximations will increase significantly. Therefore, the new MLC schemes with the directional discretization should lead to better computational efficiency in two-dimensional flow simulations.

Last, the additional degree of freedom $r$ (or $u_{xy}$) can furtherly improve the spectral resolution, which can be shown in the two-dimensional Fourier analysis in next chapter.

In summary, in the new MLC scheme with the directional discretization technique, all the 1-D upwind MLC formulas described in section II.A can be applied with no need of modification, and the 2-D central MLC formulas are not required anymore. Consequently, the new MLC scheme can overcome the inconsistency and uncertainty of the original MLC scheme, and should lead to better computational efficiency and spectral resolution.

## III. Fourier Analysis and Stability Analysis

In this chapter, the two-dimensional Fourier analysis is performed first on both the original MLC scheme and the new MLC scheme with directional discretization. The dissipation and dispersive errors, spectral resolution, and anisotropic error are analyzed and compared. Then, the matrix method is used to analyze the stability of boundary closure schemes.

### A. Two-Dimensional Fourier Analysis

The implementation of the two-dimensional Fourier analysis on the original MLC schemes are described in [1]. In this paper, the method is implemented slightly different, where the Fourier analysis is formulated as an eigenvalue problem instead of solving the roots of a polynomial. This modification makes it easier to find the modes for the new MLC scheme. For the sake of brevity, the formulation is derived briefly in this section with focus on the new MLC scheme.

The analysis is performed on the two-dimensional advection equation and its auxiliary equations, which is Eq. (22) for the new MLC scheme. To be generic, the convection angle $\theta$ and Fourier wave angle $\varphi$ are defined, and the directional convection speed in Eqs. (6) and (22) can be written as,

$$\begin{aligned} c_1 &= c \cdot \cos\theta \\ c_2 &= c \cdot \sin\theta \end{aligned} \tag{25}$$

where $c$ is the magnitude of convection speed. The Fourier mode is of the following form,

$$[u, v, w, r]^T = [\hat{u}, \hat{v}, \hat{w}, \hat{r}]^T e^{\hat{a}t + i\hat{k}(x\cos\varphi + y\sin\varphi)} \tag{26}$$

where $\hat{k}$ is the wavenumber, $\hat{a}$ is a complex characteristic parameter as a function of $\hat{k}$, and $\varphi$ is the Fourier wave angle which can be different from $\theta$. If a uniform mesh with spacing $h$ is used, the non-dimensional wavenumber $k$, the non-dimensional dissipation factor $a$, and the non-dimensional magnitude of the Fourier modes $\mathbf{U}$ can be defined as,

$$a = \frac{\hat{a}h}{c}, \quad k = \hat{k}h, \quad \mathbf{U} = \left[\hat{u}, h\hat{v}, h\hat{w}, h^2\hat{r}\right]^T \tag{27}$$

Substituting Eq. (26) into Eq. (22) and using the new MLC scheme in Eqs. (23) and (24) to discretize the spatial derivatives, an eigenvalue problem can be formulated as,

$$\mathbf{A}\mathbf{U}_{i,j} = a\mathbf{U}_{i,j} \tag{28}$$

where, $\mathbf{U}_{i,j}$ is the non-dimensional magnitude at the grid point ($i$, $j$), and $\mathbf{A}$ is an complex matrix dependent on $\theta$, $\varphi$, $k$ and the coefficients of the MLC scheme, as given below,

$$\mathbf{A} = -\cos\theta \begin{bmatrix} 0 & 1 & 0 & 0 \\ A_1 & B_1 & 0 & 0 \\ 0 & 0 & 0 & 1 \\ 0 & 0 & A_1 & B_1 \end{bmatrix} - \sin\theta \begin{bmatrix} 0 & 0 & 1 & 0 \\ 0 & 0 & 0 & 1 \\ A_2 & 0 & B_2 & 0 \\ 0 & A_2 & 0 & B_2 \end{bmatrix} \tag{29}$$

and the complex elements $A_1$, $B_1$, $A_2$, $B_2$ are,

$$\begin{aligned} A_1 &= \sum_{l=-L_1}^{L_2} a_l e^{ilk\cos\varphi}, \quad B_1 = \sum_{m=-M_1}^{M_2} b_m e^{imk\cos\varphi} \\ A_2 &= \sum_{l=-L_1}^{L_2} a_l e^{ilk\sin\varphi}, \quad B_2 = \sum_{m=-M_1}^{M_2} b_m e^{imk\sin\varphi} \end{aligned} \tag{30}$$

Four eigenvalues of $\mathbf{A}$ correspond to four modes in the two-dimensional Fourier analysis, which are the physical mode $a_1$, and three spurious modes $a_1$, $a_2$, $a_3$. The exact solution of $a$ is,

$$a_{exc} = ik\cos(\theta - \varphi) \tag{31}$$

which is an imaginary number dependent on $\theta$, $\varphi$, $k$. The real and imaginary part of modes $a_1$, $a_2$, $a_3$, $a_4$ play important roles in the Fourier analysis. It is required that $R(a_1)$ is small to reduce dissipative error, and $I(a_1)$ is close to $a_{exc}$ for small dispersive error. Meanwhile, $R(a_1)$, $R(a_2)$, $R(a_3)$, $R(a_4)$ should all be non-positive to ensure the stability of the MLC scheme.

For the original MLC scheme, the eigenvalue problem can be formulated in a similar way. The 1-D MLC scheme in Eqs. (7) and (8), and the 2-D MLC scheme in Eq.(10) are applied to the system of equations (6). The resulting matrix $\mathbf{A}$ becomes,

$$\mathbf{A} = -\cos\theta \begin{bmatrix} 0 & 1 & 0 \\ A_1 & B_1 & 0 \\ A_3 & B_3 & C_3 \end{bmatrix} - \sin\theta \begin{bmatrix} 0 & 0 & 1 \\ A_3 & B_3 & C_3 \\ A_2 & 0 & B_2 \end{bmatrix} \tag{32}$$

where $A_1$, $B_1$, $A_2$, $B_2$ still follow Eq. (30), and $A_3$, $B_3$, $C_3$ are related to the 2-D MLC scheme in Eq. (10). Their formulas are given as follows,

$$\begin{aligned} A_3 &= \sum_{\substack{l_x=-L_1 \\ l_y=-L_1}}^{L_2} a_{l_x,l_y} e^{ik\left(l_x\cos\varphi + l_y\sin\varphi\right)} \\ B_3 &= \sum_{\substack{m_x=-M_1 \\ m_y=-M_1}}^{M_2} b_{m_x,m_y} e^{ik\left(m_x\cos\varphi + m_y\sin\varphi\right)} \\ C_3 &= \sum_{\substack{n_x=-M_1 \\ n_y=-M_1}}^{M_2} c_{n_x,n_y} e^{ik\left(n_x\cos\varphi + n_y\sin\varphi\right)} \end{aligned} \tag{33}$$

Three eigenvalues of $\mathbf{A}$ correspond to one physical mode $a_1$, and two spurious modes $a_1$, $a_2$. The physical and spurious modes of the original MLC scheme are analyzed in the same way as the new MLC scheme.

In the following part of this section, the Fourier analysis results of the new MLC scheme with the directional discretization are presented, and the comparison with the original MLC scheme is given. As mentioned in the introduction, the Fourier analysis should show the minor numerical instability of the original MLC scheme.

***Fourier Analysis of the Third-Order 1-1-1-1 Scheme***

First, the third-order 1-1-1-1 scheme with $\alpha$ = 1.5 as given in Eqs. (12) and (17) is analyzed with the two-dimensional Fourier analysis. In Fig. 8, the dissipation factors of the new and original MLC schemes with different convection angle $\theta$ and Fourier wave angle $\varphi$ are compared. All modes are presented in the figures, where $R(a_1)$ is the dissipation factor of the physical mode and $R(a_2)$, $R(a_3)$, $R(a_4)$ are dissipation factors of spurious modes.

When $\theta = \varphi = 0$, as shown in Fig. 8(a), the two-dimensional Fourier analysis reduces to the one-dimensional case (see [1] for 1-D Fourier analysis). Meanwhile, the new 1-1-1-1 scheme with the directional discretization has the same behavior as the original 1-1-1-1 scheme. All modes are non-positive, which indicates both the new and original 1-1-1-1 scheme are stable. Only two distinctive modes are observed, which are a physical mode $a_1$ and a spurious mode $a_2$. The dissipative error $R(a_1)$ increases with the wavenumber $k$, and $R(a_2)$ decreases with $k$. The behaviors of $R(a_1)$ and $R(a_2)$ are favorable. If the grid resolution is good enough (small $k$) in a flow simulation, the spurious mode

should damp out due to the large dissipation factor, and the dissipative error for the physical mode should be very small. Other modes in Fig. 8(a) are trivial. The spurious mode $a_3$ in the original 1-1-1-1 scheme induced by the cross-derivative approximation are neutral ($R(a_3) = 0$), which means $a_3$ should not be changed during the simulation. For the new 1-1-1-1 scheme, $R(a_3) = R(a_1)$ and $R(a_4) = R(a_2)$ are observed, indicating that the mode $a_3$ are the same as the physical mode $a_1$ and the mode $a_4$ are equivalent with the spurious mode $a_2$.

When $\theta = 0$ and $\varphi = \pi/4$, as shown in Fig. 8(b), the dissipation factors of the 1-1-1-1 scheme are very similar with the case in Fig. 8(a). The only difference is that the physical mode is less dissipative for large $k$'s in Fig. 8(b), and the spurious mode is more dissipative on the contrary. Other observations from Fig. 8(a) keep the same for Fig. 8(b).

When $\theta = \varphi = \pi/4$, as shown in Fig. 8(c, d), the new 1-1-1-1 scheme has different behaviors from the original 1-1-1-1 scheme in the dissipation factors. The most noteworthy feature for the original scheme is the minor numerical instability of $a_1$ appearing in the neighboring region of $k = 1.75$. The magnitude of the positive part of $R(a_1)$, which equals to $10^{-3}$, is very small compared to that of a typical unstable mode. For example, in an unstable upwind MLC scheme [1], the peak of $R(a_1)$ is usually greater than 0.5. Meanwhile, the instability only appears in a very narrow range of wavenumbers. Therefore, this specific behavior is termed as the minor numerical instability. It has been proved by numerical tests that the minor numerical instability usually does not give rise to the divergence of a flow simulation [1], however, the potential risk still exists in the original MLC schemes. In the new 1-1-1-1 scheme with the directional discretization, the numerical instability is removed, and all modes become stable with non-positive dissipation factors. Meanwhile, when both $\theta$ and $\varphi$ is not zero, the physical mode $a_1$ of the new scheme is more dissipative than $a_1$ of the original scheme for large $k$'s. The spurious modes $a_2$ and $a_3$ in the new scheme overlap with $a_2$ of the original scheme. There are more distinctive modes appearing such as $a_3$ in the original scheme and $a_4$ in the new scheme. They have similar shape in the figure, however, $a_3$ of the original scheme is very close to other spurious modes, while $a_4$ of the new scheme is much more dissipative than other modes, which is related to the additional degree of freedom $u_{xy}$.

When $\theta = \pi/3$, $\varphi = \pi/6$, as shown in Fig. 8(e, f), the dissipation factors have similar features as Fig. 8(c, d) except three aspects. First, the numerical instability of the original 1-1-1-1 scheme is significantly reduced to the magnitude of $10^{-6}$, which is three orders smaller than the case in Fig. 8(d). In fact, we find that the case of $\theta = \varphi = \pi/4$ has the largest instability observed. Second, the behaviors of spurious modes become more complicated. For both the new and original 1-1-1-1 scheme, $R(a_2)$ and $R(a_3)$ are distinguishable in this case, where the latter is more dissipative. Last, all modes of the new 1-1-1-1 scheme are also distinguishable from the modes of the original 1-1-1-1 scheme, indicating that they should have different behaviors in a case where $\theta$ and $\varphi$ are not equivalent and are both non-zero.

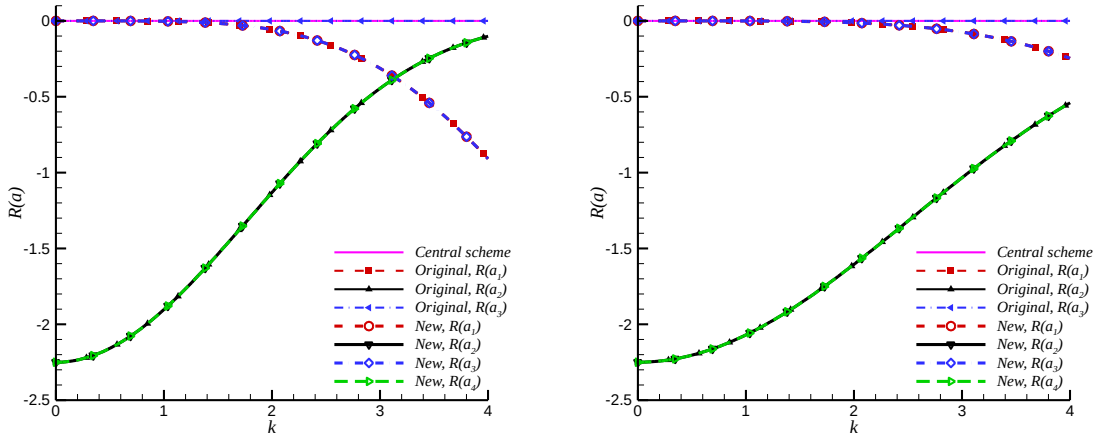


a), $\theta = 0$, $\varphi = 0$ b), $\theta = 0$, $\varphi = \pi/4$

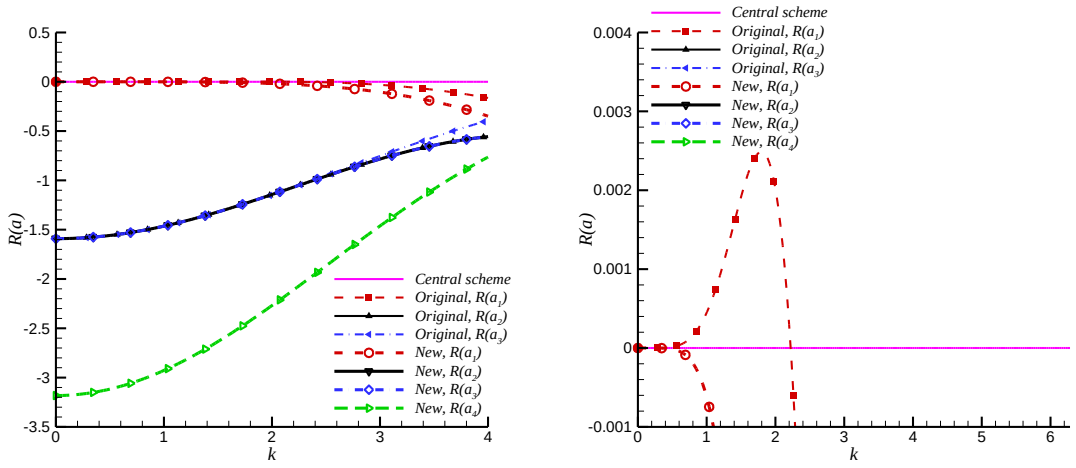


c), $\theta = \pi/4$, $\varphi = \pi/4$ d), $\theta = \pi/4$, $\varphi = \pi/4$ (zoomed-in)

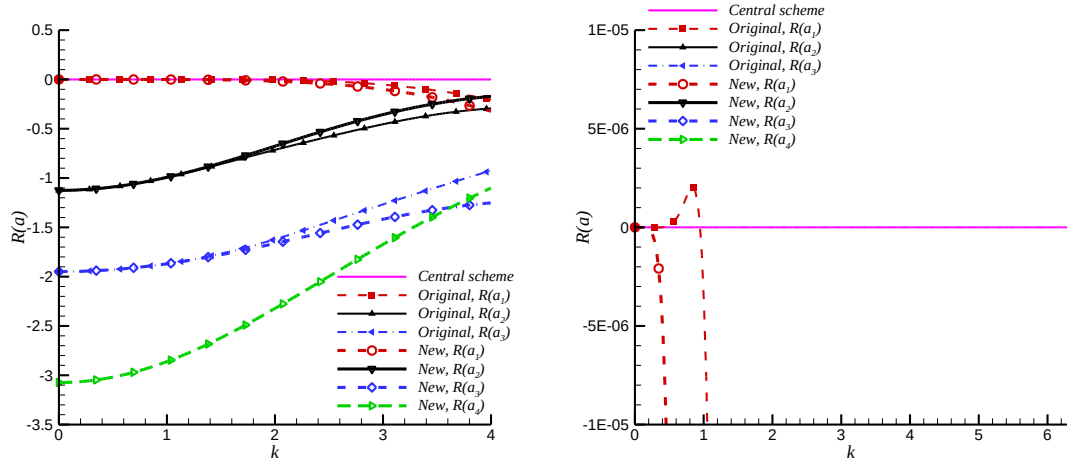


e), $\theta = \pi/3$, $\varphi = \pi/6$ f), $\theta = \pi/3$, $\varphi = \pi/6$ (zoomed-in)

**Fig. 8. Dissipation factors of the new and the original 1-1-1-1 scheme (3rd order) for two-dimensional cases.**

The modified wavenumber $I(a_1)$ of the new and the original 1-1-1-1 scheme are presented in Fig. 9. Various $\theta$ and $\varphi$ are analyzed, and the straight lines are exact solutions of $I(a)$ for different cases. When $\theta = 0$, $\varphi = 0$, the analysis reduces to the one-dimensional analysis, and the new and the original 1-1-1-1 scheme has the same modified wavenumbers. When $\theta = 0$, $\varphi = \pi/4$, the two MLC schemes also generates the same $I(a_1)$. However, in the case of $\theta = \varphi = \pi/4$ and the case of $\theta = \pi/3$, $\varphi = \pi/6$, the new 1-1-1-1 scheme has much better spectral resolution than the original 1-1-1-1 scheme. In general, the introduce of $u_{xy}$ as the additional degree of freedom can benefit the spectral resolution for the two-dimensional simulations if both $\theta$ and $\varphi$ are non-zero. A noteworthy feature of the new MLC scheme is that, the spectral resolution is better in the case of $\theta = \varphi = \pi/4$ than that in the case of $\theta = \varphi = 0$, which is consistent with most conventional finite difference methods. For the original MLC scheme, on the other hand, the spectral resolution is slightly decreased when $\theta = \varphi = \pi/4$ compared with the case of $\theta = \varphi = 0$. This difference is presented more clearly by the anisotropy analysis of phase speed in Section III.B.

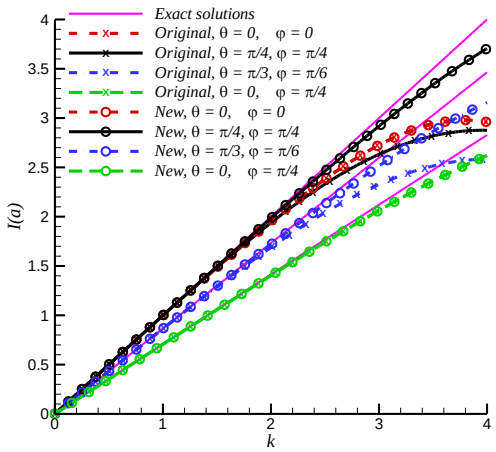


**Fig. 9. Modified wavenumber $I(a_1)$ of the new and the original 1-1-1-1 scheme (3rd order) for two-dimensional cases.**

***Fourier Analysis of the Fifth-Order 2-2-1-1 Scheme***

Then, the two-dimensional Fourier analysis is carried out to the fifth-order 2-2-1-1 scheme with $\alpha$ = -1 as given in Eqs. (14) and (18). In Fig. 10 the dissipation factors of the new and original MLC schemes with different convection angle $\theta$ and Fourier wave angle $\varphi$ are compared. Similar behaviors of all the modes as in Fig. 8 are observed for both the new and the original 2-2-1-1 scheme except the following distinction. First, all modes in Fig. 10 have much smaller dissipations for all $k$'s within the range of [0, 4], which is more significant for the spurious modes. It indicates that reducing the stencil size in the derivative layer leads to smaller dissipation in the spurious modes. This is reasonable because the conventional finite difference method without the derivative layer does not have spurious modes, or equivalently, we can think the $R(a)$ of its spurious mode reduces to zero. Second, the minor numerical instability of the original 2-2-1-1 scheme appears in both $R(a_1)$ and $R(a_3)$ when $\theta = \varphi = \pi/4$, as shown in Fig. 10(d), which is different from Fig. 8(d). For the case of $\theta = \pi/3$, $\varphi = \pi/6$, the original 2-2-1-1 scheme only generates numerical instability in $R(a_1)$, and the magnitude is much smaller than the case of $\theta = \varphi = \pi/4$. As a comparison, the new 2-2-1-1 scheme is always stable in both physical and spurious modes. Third, unusual behaviors of the spurious modes - $R(a_2)$ and $R(a_3)$ of the original 2-2-1-1 scheme is observed for small $k$'s. The $R(a_2)$ and $R(a_3)$ in Fig. 10(e) converge to a point quickly and then separate gradually. The reason behind this behavior is not clear at this moment. A possible explanation is the inconsistency of the 1-D and 2-D MLC scheme, because this unusual behavior of the spurious modes is not observed for the new 2-2-1-1 scheme, where no 2-D scheme is needed.

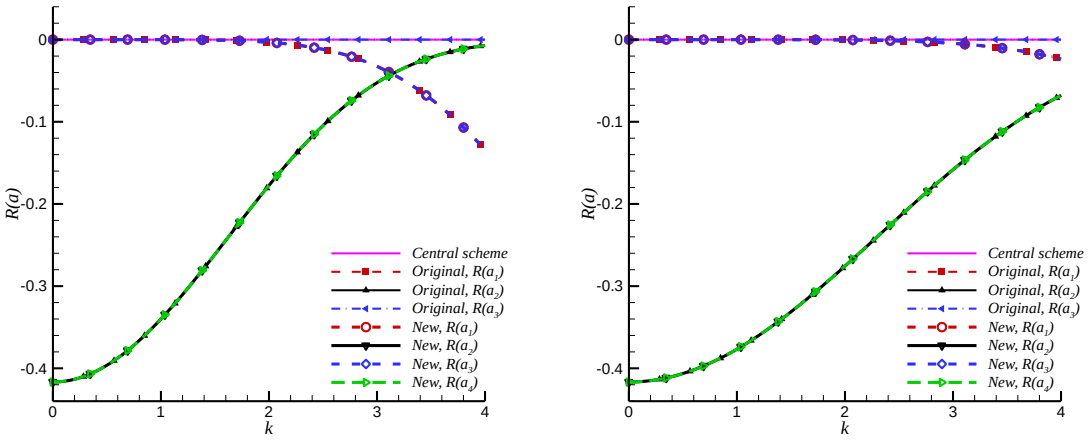


a), $\theta = 0$, $\varphi = 0$ b), $\theta = 0$, $\varphi = \pi/4$

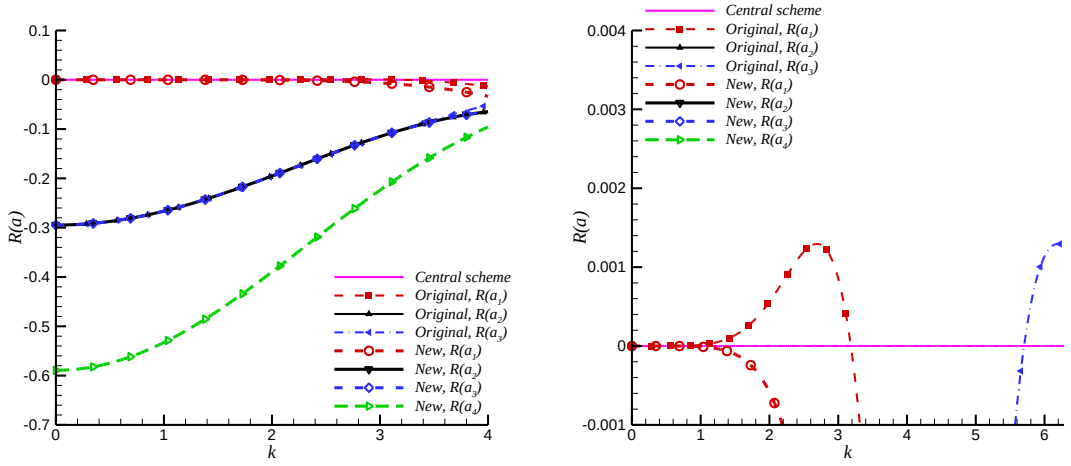


c), $\theta = \pi/4$, $\varphi = \pi/4$ d), $\theta = \pi/4$, $\varphi = \pi/4$ (zoomed-in)

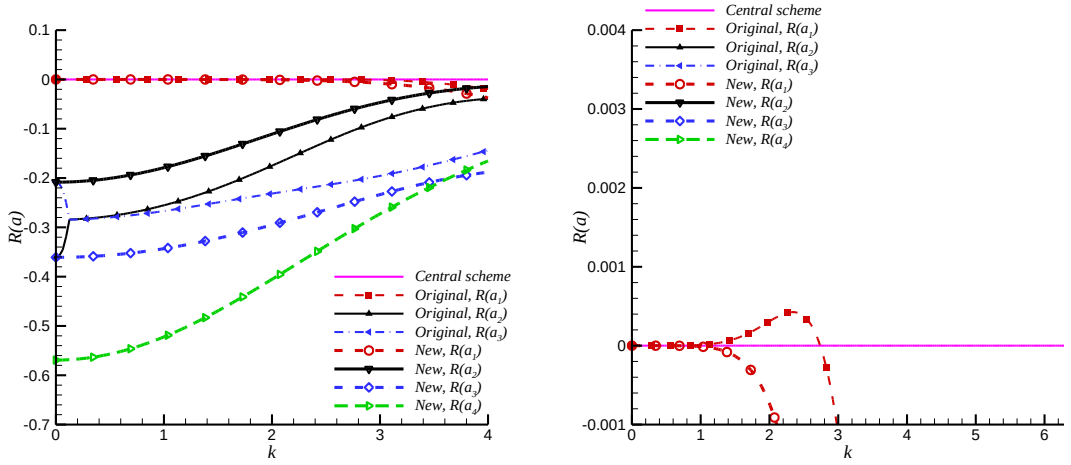


e), $\theta = \pi/3$, $\varphi = \pi/6$ f), $\theta = \pi/3$, $\varphi = \pi/6$ (zoomed-in)

**Fig. 10. Dissipation factors of the new and the original 2-2-1-1 scheme (5th order) for two-dimensional cases.**

The modified wavenumber $I(a_1)$ of the new and the original fifth-order 2-2-1-1 scheme are presented in Fig. 11. Compared with the results of third-order schemes in Fig. 9, the new 2-2-1-1 scheme shows improved resolutions in all 4 cases with different $\theta$ and $\varphi$. Similarly, the original 2-2-1-1 scheme also has better resolution than the original 1-1-1-1 scheme except that it has slightly decreased resolution for large wavenumbers in the case of $\theta = \pi/3$ and $\varphi = \pi/6$.

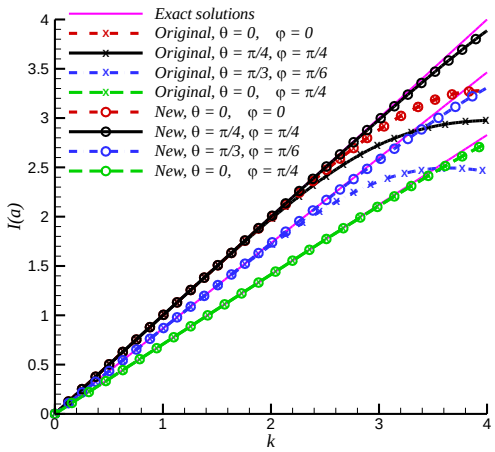


**Fig. 11. Modified wavenumber $I(a_1)$ of the new and the original 2-2-1-1 scheme (5th order) for two-dimensional cases.**

***Fourier Analysis of the Seventh-Order 2-2-2-2 Scheme***

Finally, the two-dimensional Fourier analysis is carried out to the seventh-order 2-2-2-2 scheme with $\alpha = 12$ as given in Eqs. (16) and (19). The dissipation factors of the new and original MLC schemes are given in Fig. 12, and the modified wavenumbers are given in Fig. 13. Again, various convection angle $\theta$ and Fourier wave angle $\varphi$ are compared. The Fourier analysis results of the seventh-order schemes are very similar to the third- and fifth-order schemes. Compared with the third-order 1-1-1-1 scheme, both the new and the original 2-2-2-2 scheme has smaller dissipation and better spectral resolutions. The numerical instability of the original 2-2-2-2 scheme observed in Fig. 12(d, f) has larger magnitude than that of the 1-1-1-1 scheme, which means it is less stable. Again, the case of $\theta = \varphi = \pi/4$ shows much larger instability than the case of $\theta = \pi/3$, $\varphi = \pi/6$. On the other hand, the new 2-2-2-2 scheme with the directional discretization is always stable.

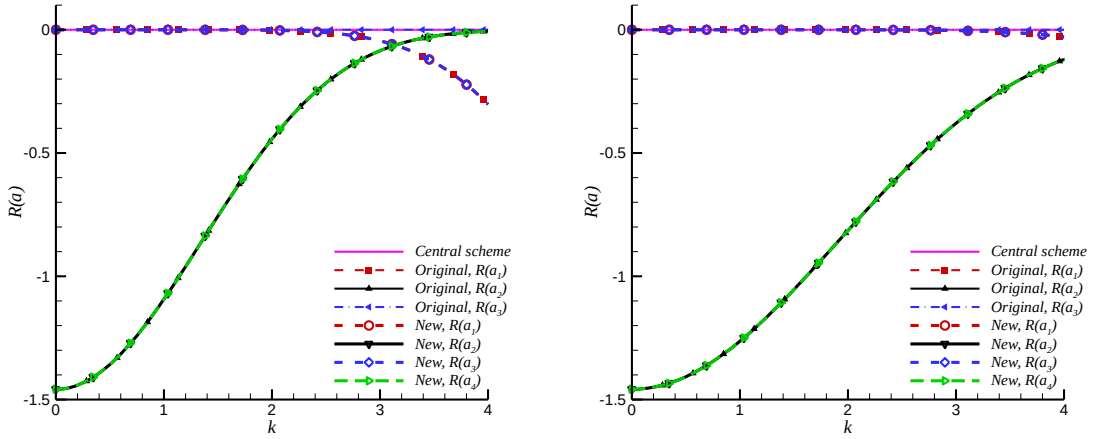


a), $\theta = 0$, $\varphi = 0$ b), $\theta = 0$, $\varphi = \pi/4$

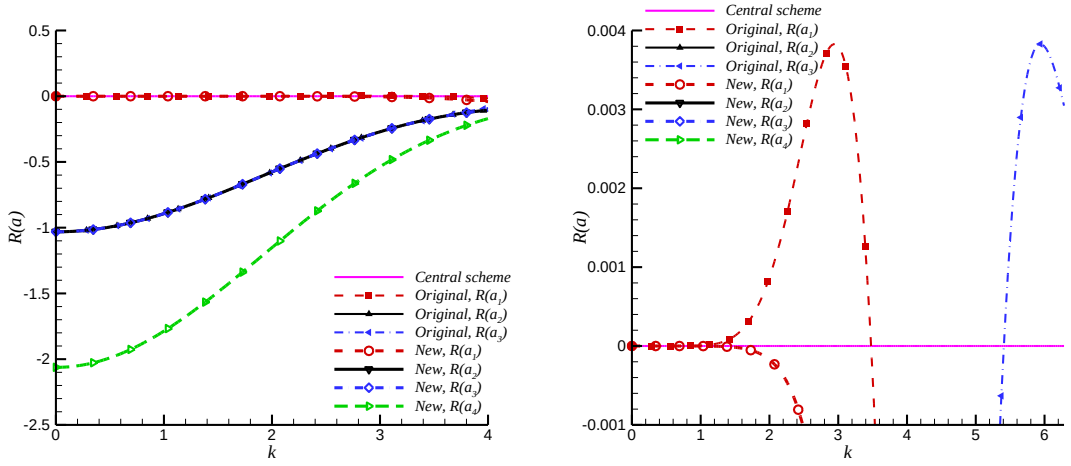


c), $\theta = \pi/4$, $\varphi = \pi/4$ d), $\theta = \pi/4$, $\varphi = \pi/4$ (zoomed-in)

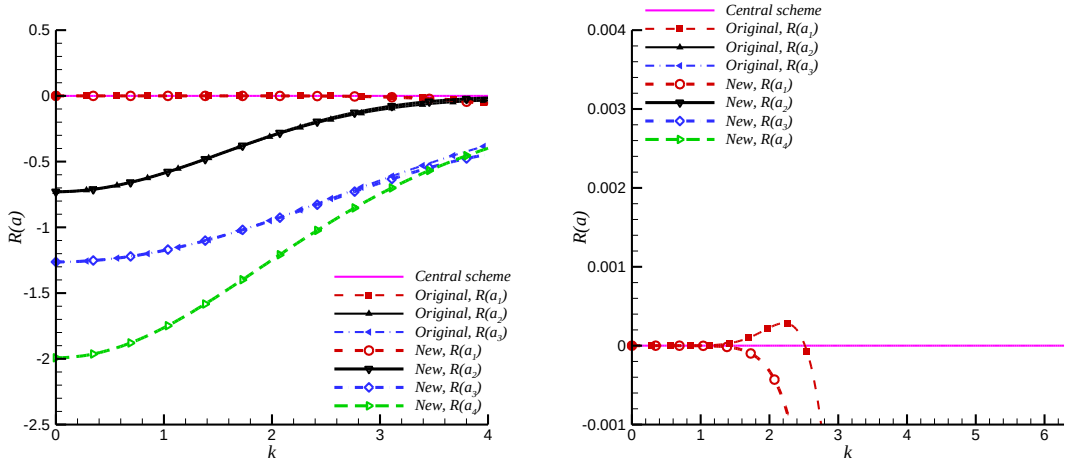


e), $\theta = \pi/3$, $\varphi = \pi/6$ f), $\theta = \pi/3$, $\varphi = \pi/6$ (zoomed-in)

**Fig. 12. Dissipation factors of the new and the original 2-2-2-2 scheme (7th order) for two-dimensional cases.**

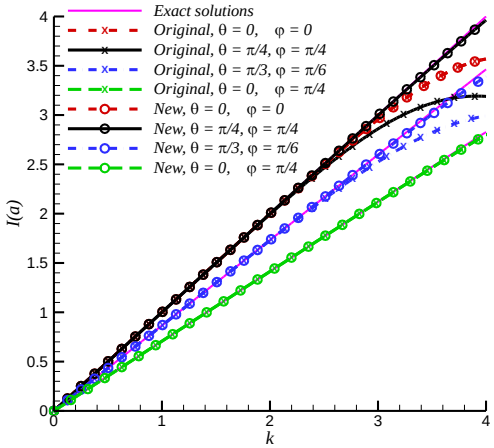


**Fig. 13. Modified wavenumber $I(a_1)$ of the new and the original 2-2-2-2 scheme (7th order) for two-dimensional cases.**

A summary of the Fourier analysis above is given to end this section:

1. The new and original MLC schemes have the same dissipation factors and modified wavenumbers when $\theta = 0$, and both reduces to the one-dimensional case when $\theta = \varphi = 0$.
2. When $\theta$ and $\varphi$ are non-zero, the new and the original MLC schemes both become more complicated and show different behaviors. Specifically, the new MLC scheme has slightly larger dissipation than the original MLC scheme for large wavenumbers in the physical mode, and the new scheme also generates an additional spurious mode which is significantly more dissipative than other modes for small wavenumbers.
3. The original MLC scheme shows minor numerical instabilities when both $\theta$ and $\varphi$ is non-zero, where the case of $\theta = \varphi = \pi/4$ generates the largest instability. Increasing the order of accuracy usually leads to more numerical instability. On the other hand, the new MLC scheme is always stable because no 2-D MLC scheme is required benefited from the directional discretization technique.
4. When both $\theta$ and $\varphi$ is non-zero, the new MLC scheme shows much better spectral resolution than the original MLC scheme because of the additional degree of freedom $u_{xy}$.
5. For both the new and original MLC scheme, increasing the order of accuracy leads to smaller dissipation and higher spectral resolution. On the other hand, the MLC scheme is greatly affected by the stencil size of the derivative layer, where a narrower stencil for derivatives can leads to a much less dissipative MLC scheme.

## B. Anisotropy Analysis of the Phase Speed

In this section, the anisotropy analysis is performed following the same approach as in the two-dimensional Fourier analysis. To investigate the anisotropic error of the MLC schemes, the phase speed $c_p$ is computed from the modified wavenumber $I(a_1)$,

$$c_p(k,\theta) = \frac{I(a_1)}{k} \tag{34}$$

where $I(a_1)$ is a function of wavenumber $k$, convection angle $\theta$, and Fourier wave angle $\varphi$. Here, we follow Lele's approach [5] in the anisotropy analysis by assuming $\varphi = \theta$, so that $c_p$ is only dependent on $k$ and $\theta$.

Fig. 14 compares the phase speed $c_p$ of the new and original MLC schemes. The $c_p$ contours are plotted in the range of $k = [0, 2\pi]$ and $\theta = [0, 2\pi]$, where each curve represents the $c_p$ value for different $\theta$ and a constant $k$. The exact value of $c_p$ is 1 for any $k$ and $\theta$, which corresponds to the outermost circle in the plots. Two properties can be analyzed from the figure; the distorted shape from a perfect circle represents the anisotropic error, and the shrink of the circle represents the dispersive error. Small $k$ values correspond to outer contours, and large $k$ values are represented by inner contours. The figures show that both the anisotropic and dispersive errors increase as $k$ increases from 0 to $2\pi$. Comparing the new and original MLC schemes with the same order of accuracy, we find that the new scheme always has smaller dispersive error than the original scheme. Meanwhile, the new MLC scheme also shows smaller anisotropic error for a large portion of the wavenumbers in $[0, 2\pi]$. Only when $k$ is very large (contours close to the center), the original MLC scheme shows better isotropy. This advantage of the MLC scheme on the isotropy becomes more significant when the order of accuracy increases. For example, the new 2-2-2-2 scheme in (c) shows much smaller anisotropic error than the original 2-2-2-2 scheme in (f) for $k < 1.6\pi$ (outside the orange dashed line). The small $k$ components are usually dominating and more important in flow simulations. Therefore, the new MLC scheme should possess better numerical isotropy than the original MLC scheme for two-dimensional cases.

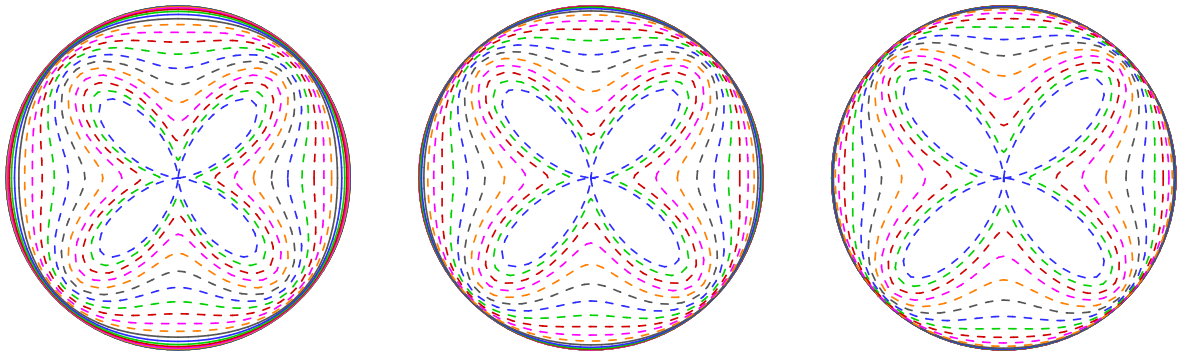

a) b) c)

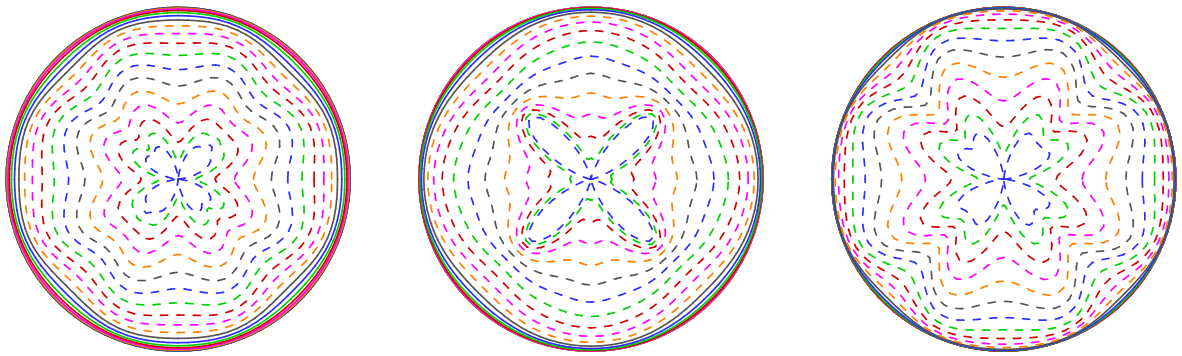

d) e) f)

**Fig. 14. Polar plot of $c_p$ for the new and original MLC schemes (contours are plotted at $k/\pi$ = 1/50, 5/50, …, 45/50, 50/50 with solid lines, and 55/50, …, 100/50 with dashed lines): a), New third-order 1-1-1-1 scheme; b), New fifth-order 2-2-1-1 scheme; c), New seventh-order 2-2-2-2 scheme; d), Original third-order 1-1-1-1 scheme; e), Original fifth-order 2-2-1-1 scheme; f), Original seventh-order 2-2-2-2 scheme.**

It is also noteworthy that the contours of the new and original MLC schemes possess different patterns. The new schemes in Fig. 14(a, b, c) always have the smallest dispersive error at $\theta = \pm\pi/4$ and $\pm 3\pi/4$, and the largest error at $\theta = 0$, $\pi$, and $\pm\pi/2$. While the original schemes in Fig. 14(d, e, f) have more complicated patterns. Specifically, the original 1-1-1-1 scheme and the original 2-2-2-2 scheme have similar patterns where the smallest dispersive error seems to appear at $\theta = \pm\pi/8$, $\pm 3\pi/8$, $\pm 5\pi/8$, $\pm 7\pi/8$, and the largest error seems to locate at $\theta = 0$, $\pi$, and $\pm\pi/2$. The original 2-2-1-1 scheme presents an unclear pattern in the contours; a possible reason is that the stencil size for the value layer and the derivative layer are different.

The complex pattern of the original MLC schemes is due to the inconsistency between the 1-D and 2-D MLC scheme. As mentioned in Section II.A, the formulas for second derivatives and cross derivatives are derived separately in the original MLC scheme, and the upwind setting is applied to second derivatives only. On the other hand, the new MLC scheme can use the same formula for all derivatives through the directional discretization technique; therefore, the upwind scheme can apply to the entire system. An evidence is from the anisotropy analysis for conventional finite difference methods. In Fig. 15, the phase speed $c_p$ of Zhong's fifth-order upwind explicit scheme with $\alpha$ = -6, and Zhong's fifth-order upwind compact scheme with $\alpha$ = -1 [50] are analyzed in a similar way. Because a mono-layer scheme cannot resolve any wave with $k > \pi$, only $k$ within $[0, \pi]$ is plotted. It is clearly that the both Zhong's explicit scheme and compact scheme in Fig. 15 shows the same pattern as the new MLC scheme in Fig. 14(a, b, c), although these conventional schemes have much lower spectral resolution due to their the mono-layer framework. This similarity indicates that with the directional discretization, the new MLC schemes can achieve consistency in the multi-layer framework.

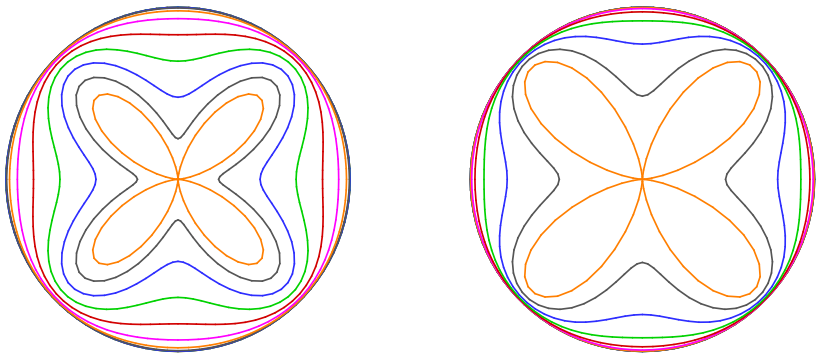

a) b)

**Fig. 15. Polar plot of $c_p$ for conventional finite difference methods (contours are plotted at $k/\pi$ = 1/50, 5/50, …, 45/50, 50/50): a), Zhong's fifth-order explicit scheme; b), Zhong's fifth-order compact scheme.**

In summary, the anisotropy analysis demonstrates that the new MLC scheme has better isotropic phase speed than the original MLC scheme in two-dimensional cases. Through the directional discretization technique, the

dispersive error along any orientation is reduced for wavenumbers within the range of [0, 2π], and the anisotropic error is reduced for a large portion of wavenumbers in [0, 2π]. The new MLC scheme can also achieve the consistency in the multi-layer framework. Accordingly, it has a simple and clear pattern in the anisotropy contours as the conventional finite difference method does, while the original MLC scheme shows more complicated patterns.

### C. Stability of Boundary Closure Schemes in Two-Dimensional Cases

High-order finite difference methods often require boundary closure schemes for grid points on or near the boundaries of the computational domain. When the inner scheme is coupled with boundary closure schemes, the stability of the inner scheme can be affected. It is known that for a *p*-th-order inner scheme, the stable boundary closure scheme can be one order lower to maintain the *p*-th-order global accuracy of the inner scheme. The analysis for boundary closure schemes in the one-dimensional cases have been finished through the matrix method in [1], and the stable configuration has been obtained for the original 1-1-1-1 scheme and 2-2-2-2 scheme. The matrix method used in the one-dimensional analysis can be generalized to the two-dimensional stability analysis.

The two-dimensional advection equation and its auxiliary equations as shown in Eqs. (6) and (22) are used again in the matrix method. A finite domain is discretized by a uniform mesh with grid spacing $h$ in both $x$ and $y$ direction, as shown in Fig. 16. Both $x$ and $y$ are in the range of [0, $Nh$], i.e., the indexes $i$ and $j$ arrange from 0 to $N$. Inflow boundary conditions are used at $i = 0$ and $j = 0$, and characteristic boundary condition is used at $i = N$ and $j = N$. For the linear advection, the inflow conditions are specified by $u^j{}_0(x, t)$ and $u^i{}_0(y, t)$; the characteristic boundary conditions are implemented by using one-sided MLC scheme. The upwind MLC schemes on centered stencil are used at interior grid points, and different boundary closure schemes are applied when the stencil of inner scheme goes beyond the left and right boundaries. For the original MLC schemes, specific formulas of boundary closure schemes for cross derivatives are selected carefully, though it may not be the optimal choice due to the uncertainty in cross derivatives. For the new MLC schemes, both the 1-D inner scheme and the 1-D boundary closure scheme can be extended to two-dimensional cases naturally without extra derivations.

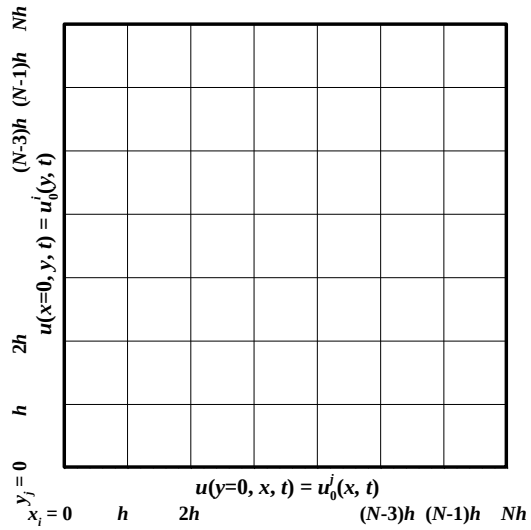


**Fig. 16. Schematic for stability analysis on two-dimensional linear advection equation.**

In the matrix method, Eq. (6) or Eq. (22) is discretized into a system of ordinary differential equations by using the inner and boundary closure schemes. By assuming $c = 1$ and defining the convection angle $\theta$, $c_1$ and $c_2$ in Eqs. (6) and (22) can be replaced by $\cos\theta$ and $\sin\theta$ respectively. The resulting equations can be written in a system of ordinary differential equations in matrix form,

$$\frac{d}{dt}\overline{\mathbf{U}} = \mathbf{L}\cdot\overline{\mathbf{U}} + \mathbf{G}(t) \tag{35}$$

where $\mathbf{G}(t)$ is the matrix containing all the boundary source terms, and it can be ignored in the stability analysis. The first normal derivatives and cross derivatives on the inflow boundary can be determined from the two-dimensional advection equation as follows,

$$
\begin{aligned}
u_y\left(x, y=0, t\right) &= -\frac{1}{c_2}\left[c_1 u_x\left(x, y=0, t\right) + u_t\left(x, y=0, t\right)\right] \\
u_{xy}\left(x, y=0, t\right) &= -\frac{1}{c_2}\left[c_1 u_{xx}\left(x, y=0, t\right) + u_{xt}\left(x, y=0, t\right)\right] \\
u_x\left(x=0, y, t\right) &= -\frac{1}{c_1}\left[c_2 u_y\left(x=0, y, t\right) + u_t\left(x=0, y, t\right)\right] \\
u_{xy}\left(x=0, y, t\right) &= -\frac{1}{c_1}\left[c_2 u_{yy}\left(x=0, y, t\right) + u_{yt}\left(x=0, y, t\right)\right]
\end{aligned}
\tag{36}
$$

where the temporal derivative on the right-hand side is prescribed and other terms can be calculated analytically or approximated locally on the boundaries. If the new MLC scheme is applied, $\overline{\mathbf{U}}$ and $\mathbf{L}$ in Eq. (35) have the form,

$$
\overline{\mathbf{U}} = \left(\mathbf{U}, \mathbf{U_x}, \mathbf{U_y}, \mathbf{U_{xy}}\right)^T, \quad \mathbf{L} = -\begin{bmatrix} \mathbf{0} & \mathbf{I}\cos\theta & \mathbf{I}\sin\theta & \mathbf{0} \\ \mathbf{A}_1\cos\theta & \mathbf{B}_1\cos\theta & \mathbf{0} & \mathbf{I}\sin\theta \\ \mathbf{A}_2\sin\theta & \mathbf{0} & \mathbf{B}_2\sin\theta & \mathbf{I}\cos\theta \\ \mathbf{0} & \mathbf{A}_2\sin\theta & \mathbf{A}_1\cos\theta & \mathbf{B}_1\cos\theta + \mathbf{B}_2\sin\theta \end{bmatrix} \tag{37}
$$

where $\mathbf{U}$, $\mathbf{U_x}$, $\mathbf{U_y}$, $\mathbf{U_{xy}}$ are vectors containing all the unknowns at the grid points, and matrices $\mathbf{A_1}$, $\mathbf{A_2}$ and $\mathbf{B_1}$, $\mathbf{B_2}$ consist of the coefficients of both the 1-D inner scheme and 1-D boundary closure schemes. If the original MLC scheme is applied, $\overline{\mathbf{U}}$ and $\mathbf{L}$ in Eq. (35) have the form,

$$
\overline{\mathbf{U}} = \left(\mathbf{U}, \mathbf{U_x}, \mathbf{U_y}\right)^T, \quad \mathbf{L} = -\begin{bmatrix} \mathbf{0} & \mathbf{I}\cos\theta & \mathbf{I}\sin\theta \\ \mathbf{A}_1\cos\theta + \mathbf{C}\sin\theta & \mathbf{B}_1\cos\theta + \mathbf{D}\sin\theta & \mathbf{E}\sin\theta \\ \mathbf{A}_2\sin\theta + \mathbf{C}\cos\theta & \mathbf{D}\cos\theta & \mathbf{B}_2\sin\theta + \mathbf{E}\cos\theta \end{bmatrix} \tag{38}
$$

where matrices $\mathbf{A_1}$, $\mathbf{A_2}$ and $\mathbf{B_1}$, $\mathbf{B_2}$ keep the same and $\mathbf{C}$, $\mathbf{D}$, and $\mathbf{E}$ contain the coefficients of both the 2-D inner scheme and 2-D boundary closure schemes. The dimension of the vectors and matrices are as follows,

$$
\mathbf{U},\ \mathbf{U_x},\ \mathbf{U_y},\ \mathbf{U_{xy}} \in R^{N^2}, \qquad \mathbf{I},\ \mathbf{A}_1,\ \mathbf{A}_2,\ \mathbf{B}_1,\ \mathbf{B}_2,\ \mathbf{C},\ \mathbf{D},\ \mathbf{E} \in R^{N^2 \times N^2} \tag{39}
$$

The stability of Eq. (35) is determined by eigenvalue of matrix $\mathbf{L}$, which only depends on the particular inner and boundary closure schemes. For asymptotic stability, the real part of all the eigenvalues of $\mathbf{L}$ needs to be non-positive. In this paper, the eigenvalues of $\mathbf{L}$ are solved numerically, and the eigenvalue spectrum is used to show stability. Different $\alpha$ values for the 1-D inner scheme are analyzed.

From the stability analysis of boundary closure schemes in the one-dimensional cases [1], two stable configurations of inner and boundary closure schemes are obtained, which are listed in Table 1. In this section, the configuration is extended to two-dimensional cases. For the new MLC scheme with the spatial discretization, no extra derivation is needed. For the original MLC scheme, the additional configuration for the cross derivatives are listed in Table 2. Note that inflow boundary conditions are applied on $i = 0$ and $j = 0$, where the values and tangential derivatives are prescribed and the normal derivatives are determined from Eq. (36). From the configurations in Table 1 and Table 2, it is expected that Case 1 have the third-order global accuracy and Case 2 have the seventh-order global accuracy. Both the 1-D and 2-D inner schemes are presented in Section II.A. The formulas for the 1-D boundary closure schemes can be found in [1], and the formulas for the 2-D boundary closure schemes are given in Appendix.

**Table 1. Selection of the 1-D inner schemes and 1-D boundary closure schemes for second derivatives.**

| Case 1: 3rd-order global accuracy | Case 2: 7th-order global accuracy |
|---|---|
| *i (j)* = 1 to *N*-1: 3rd-order 1-1-1-1 scheme<br>*i (j)* = *N*: 3rd-order 2-0-1-0 scheme | *i (j)* = 1: 6th-order 1-2-1-2 scheme<br>*i (j)* = 2 to *N*-2: 7th-order 2-2-2-2 scheme<br>*i (j)* = *N*-1: 6th-order 2-1-2-1 scheme<br>*i (j)* = *N*: 6th-order 3-0-3-0 scheme |

**Table 2. Selection of the 2-D inner schemes and 2-D boundary closure schemes for cross derivatives.**

| | | Scheme configuration | | | |
|---|---|---|---|---|---|
| | | *i* = 1 to *N*-1 | | *i* = *N* | |
| Case 1 | *j* = 1 to *N*-1 | 4th | | 3rd | |
| | *j* = *N* | 3rd | | 2nd | |
| | | *i* = 1 | *i* = 2 to *N*-2 | *i* = *N*-1 | *i* = *N* |
| Case 2 | *j* = 1 | 6th | 6th | 6th | 6th |
| | *j* = 2 to *N*-2 | 6th | 8th | 6th | 6th |
| | *j* = *N*-1 | 6th | 6th | 6th | 6th |
| | *j* = *N* | 6th | 6th | 6th | 6th |

Fig. 17 shows the eigenvalue spectrum for Case 1, where the overall order of accuracy is 3. The eigenvalue spectrums show that the third-order configuration in both the new and original MLC schemes are stable with all three $\alpha$ values. Both figures show that larger $\alpha$ causes the spectrum to move towards negative direction, which means the scheme becomes more stable. When $\alpha$ = 3, a large portion of the eigenvalue spectrum is significantly shifted to the negative direction, which indicates there may be excessive dissipation. As we suggested in the one-dimensional analysis [1], $\alpha$ = 1.5 is a reasonable choice for introducing small but enough dissipation. Fig. 17 also shows that the new MLC scheme (b) has a more coherent pattern in the eigenvalue spectrum compared with the original MLC scheme (a). The new MLC scheme has more concentrated eigenvalue spectrum for each specific $\alpha$ value, and the spectrums for different $\alpha$ values are better separated.

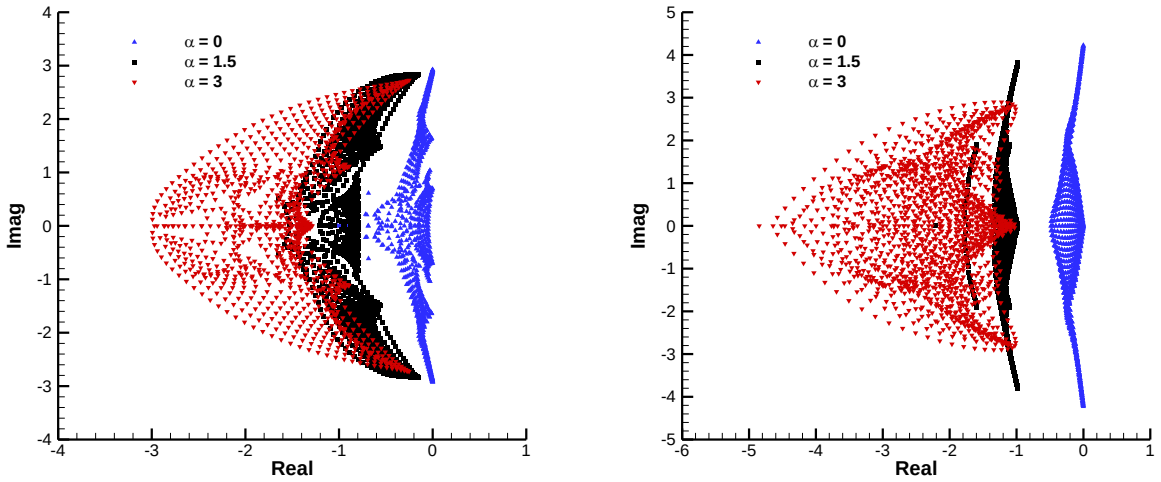


a), original 1-1-1-1 scheme

b), new 1-1-1-1 scheme

**Fig. 17. Comparison of the eigenvalue spectrum for Case 1 (3rd-order global accuracy) with the original and new MLC schemes.**

Similarly, Fig. 18 shows the eigenvalue spectrum for Case 2, where the overall order of accuracy is 7. Fig. 18(a) shows that the seventh-order configuration with $\alpha$ = 0, 12, 24 for the 1-D inner scheme are unstable in the original MLC scheme. Only $\alpha$ = 36 leads to non-positive real parts in the eigenvalue spectrum, which indicates that the original MLC scheme requires a very large $\alpha$ to insure boundary stability in Case 2. Fig. 18(b) shows the seventh-order configuration with $\alpha$ = 12, 24, 36 are all stable, indicating that the boundary stability is much easier to achieve in the new MLC scheme with the directional discretization. For maintaining small dissipation, $\alpha$ = 12 is a reasonable choice. Similar to Case 1 in Fig. 17, the new MLC scheme also shows more concentrated and better separated eigenvalue spectrums for Case 2 compared with the original MLC scheme.

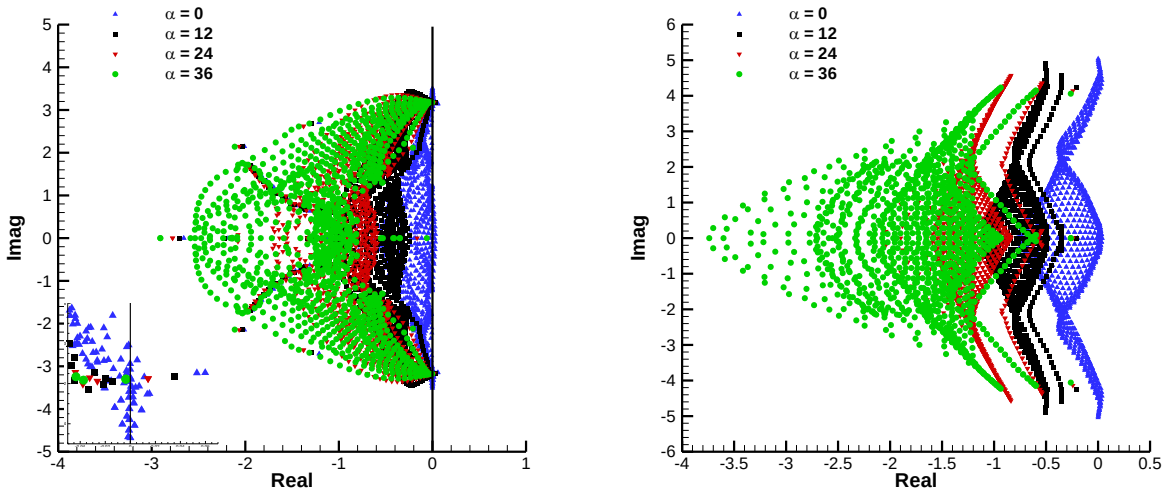


a), original 2-2-2-2 scheme

b), new 2-2-2-2 scheme

**Fig. 18. Comparison of the eigenvalue spectrum for Case 2 (7th-order global accuracy) with the original and new MLC scheme.**

In summary, the analysis of boundary closure schemes in two-dimensional cases demonstrates that stable boundary closure schemes can be obtained in both the new and original MLC schemes by choosing a reasonable $\alpha$. However, in the case of very high-order inner scheme such as the 2-2-2-2 scheme, the new MLC scheme shows much better boundary stability for small $\alpha$ values; while the original 2-2-2-2 scheme requires very large $\alpha$ values, which introduce too much dissipation.

Chapter 3 compared the new MLC scheme and the original MLC scheme with the two-dimensional Fourier analysis and matrix method. By using the directional discretization technique, the new scheme is consistent in one- and two-dimensional cases, and it overcomes the uncertainty arising from the approximation of cross derivatives. The results demonstrate that the new MLC scheme can avoid the minor numerical instability encountered in the original MLC scheme, and it also has better spectral resolution and smaller anisotropic error for a large portion of wavenumbers in $[0, 2\pi]$ compared with the original scheme. When coupled with the boundary closure schemes, the new MLC scheme also shows better stability than the original scheme, which allows using smaller $\alpha$ values to avoid excessive dissipation.

## IV. Numerical Tests of MLC Schemes

In this chapter, the numerical tests are conducted for the 2-D linear advection, the 2-D entropy wave, and the 2-D isentropic vortex problems. Both the new and the original MLC schemes are applied to these tests, and Zhong's upwind explicit scheme are also used for comparison in some cases. The adjustable parameter $\alpha$ for MLC schemes follows the recommended values in [1], which are also given in Section II.A. Numerical solutions are compared with corresponding analytical solutions, and the order of accuracy is evaluated by grid refinement. Periodic boundary conditions are set for most cases in this chapter. In the 2-D linear advection, the effect of boundary closure schemes for non-periodic boundaries is also investigated.

### A. Linear Advection Equation

In this section, the propagation of a sinusoidal plane wave is simulated, which is governed by Eq. (5). The exact solution and initial condition of the wave ($t = 0$) are given as,

$$u(x, y, t) = 2\sin\left[6\pi\left(x + y - (c_1 + c_2)t\right) + 0.5\right] \tag{40}$$

where $c_1$ and $c_2$ are the directional advection speeds in Eq. (5), and both is set to be $\sqrt{2}/2$ here. The setting is consistent with the case of $\theta = \varphi = \pi/4$ in the two-dimensional Fourier analysis (see Fig. 8, Fig. 10, and Fig. 12, where the minor numerical stability exists.

The computational domain is a square field within the range of $0 < x < 1$ and $0 < y < 1$, which includes three wave periods. A uniform mesh with $N$ grid panels in both dimensions is used. If the periodic boundary condition is

applied, only the inner MLC scheme is needed for spatial discretization. If the non-periodic boundary condition is used, both the inner MLC scheme and boundary closure schemes are needed. The scheme configuration and spatial discretization for the non-periodic case are described in Table 1 and Table 2. The original MLC scheme, the new MLC scheme, and Zhong's upwind explicit scheme are tested in this example. The system of equations (6) is used for the original MLC scheme; the system of equations (22) is used for the new MLC scheme; and Zhong's upwind explicit scheme applies to the original equation (5) directly. The fourth-order Runge-Kutta method is used for the time integration. A small CFL number of 0.01 is used, so that the error from the time integration is much smaller than that from the spatial discretization.

***Results of Periodic Boundary Conditions***

In the first place, the periodic boundary conditions are applied to all boundaries. The solution at $t = 1$ from the original and new MLC schemes are compared to show the errors and rates of convergence. The results of the third-order 1-1-1-1 scheme, the fifth-order 2-2-1-1 scheme, and the seventh-order 2-2-2-2 scheme are presented in Table 3, Table 4 and Table 5. The rates of convergence demonstrate that both the original MLC scheme and the new MLC scheme can achieve their expected orders of accuracy. For the original scheme, the rates of convergence are even higher than the expected order. The higher convergence rate is related to the central scheme for cross-derivative approximations. Compared with the upwind scheme for second derivatives, the central scheme is one order higher in accuracy, while the expected order is determined by the upwind scheme. For the new MLC scheme with the directional discretization, the rates of convergence are closer to the expected order because only the 1-D upwind scheme is used in the spatial discretization. On the other hand, the new MLC scheme outperforms the original MLC scheme with respect to accuracy, because it always shows smaller error on the same mesh. The difference in error is more obvious when $N$ is small, which corresponds to large wavenumbers in the Fourier analysis (see Fig. 9, Fig. 11, and Fig. 13). In other words, both the numerical test and Fourier analysis prove that the new MLC scheme has better spectral resolution for large wavenumbers because of its additional degree of freedom $u_{xy}$. Moreover, this advantage of the new scheme on accuracy becomes more significant for very high-order schemes like the 2-2-1-1 scheme in Table 4 and the 2-2-2-2 scheme in Table 5, where the error of the new scheme is always one order smaller than the error of the original scheme. Since the main purpose to develop the MLC scheme is to achieve both the very high-order of accuracy and the spectral-like resolution, the new scheme developed in this paper could further realize the goal in two-dimensional flow simulations.

**Table 3. Errors and rates of convergence of the original and new 1-1-1-1 scheme (3rd order) for 2-D linear advection with periodic boundary conditions ($t = 1$).**

| $N$ | Original 1-1-1-1 scheme, $\alpha = 1.5$ | | | | New 1-1-1-1 scheme, $\alpha = 1.5$ | | | |
|---|---|---|---|---|---|---|---|---|
| | $L_1$ error | Order | $L_2$ error | Order | $L_1$ error | Order | $L_2$ error | Order |
| 10 | 2.23E+00 | \ | 2.46E+00 | \ | 7.59E-01 | \ | 8.32E-01 | \ |
| 20 | 2.22E-01 | 3.33 | 2.46E-01 | 3.32 | 9.50E-02 | 3.00 | 1.06E-01 | 2.98 |
| 40 | 1.20E-02 | 4.21 | 1.33E-02 | 4.21 | 7.97E-03 | 3.57 | 8.85E-03 | 3.58 |
| 80 | 6.38E-04 | 4.23 | 7.09E-04 | 4.23 | 5.54E-04 | 3.85 | 6.16E-04 | 3.84 |
| 160 | 3.72E-05 | 4.10 | 4.14E-05 | 4.10 | 3.58E-05 | 3.95 | 3.98E-05 | 3.95 |

**Table 4. Errors and rates of convergence of the original and new 2-2-1-1 scheme (5th order) for 2-D linear advection with periodic boundary conditions ($t = 1$).**

| $N$ | Original 2-2-1-1 scheme, $\alpha = -1$ | | | | New 2-2-1-1 scheme, $\alpha = -1$ | | | |
|---|---|---|---|---|---|---|---|---|
| | $L_1$ error | Order | $L_2$ error | Order | $L_1$ error | Order | $L_2$ error | Order |
| 10 | 1.63E+00 | \ | 1.86E+00 | \ | 1.00E-01 | \ | 1.10E-01 | \ |
| 20 | 4.18E-02 | 5.28 | 4.63E-02 | 5.33 | 2.02E-03 | 5.63 | 2.25E-03 | 5.61 |
| 40 | 6.96E-04 | 5.91 | 7.74E-04 | 5.90 | 4.98E-05 | 5.34 | 5.54E-05 | 5.35 |
| 80 | 1.08E-05 | 6.01 | 1.20E-05 | 6.01 | 1.32E-06 | 5.24 | 1.47E-06 | 5.24 |
| 160 | 1.55E-07 | 6.12 | 1.73E-07 | 6.12 | 3.13E-08 | 5.40 | 3.48E-08 | 5.40 |

**Table 5. Errors and rates of convergence of the original and new 2-2-2-2 scheme (7th order) for 2-D linear advection with periodic boundary conditions ($t = 1$).**

| $N$ | Original 2-2-2-2 scheme, $\alpha = 12$ | | | | New 2-2-2-2 scheme, $\alpha = 12$ | | | |
|---|---|---|---|---|---|---|---|---|
| | $L_1$ error | Order | $L_2$ error | Order | $L_1$ error | Order | $L_2$ error | Order |
| 10 | 7.75E-01 | \ | 8.59E-01 | \ | 2.69E-02 | \ | 2.95E-02 | \ |
| 20 | 4.99E-03 | 7.28 | 5.54E-03 | 7.27 | 1.85E-04 | 7.18 | 2.06E-04 | 7.16 |
| 40 | 1.82E-05 | 8.10 | 2.02E-05 | 8.10 | 1.18E-06 | 7.29 | 1.31E-06 | 7.29 |
| 80 | 4.93E-08 | 8.53 | 5.48E-08 | 8.52 | 6.21E-09 | 7.58 | 6.89E-09 | 7.57 |
| 160 | 1.16E-10 | 8.73 | 1.29E-10 | 8.73 | 3.53E-11 | 7.46 | 3.92E-11 | 7.46 |

To investigate the accuracy and stability of the MLC schemes, the long-time simulation results at $t$ = 100 after the sinusoidal wave has traveled approximate 212 wavelengths are analyzed. The computational efficiency of different MLC schemes is compared as well. Fig. 19 compares the evolution of $L_2$ error with non-dimensional grid spacing $\beta$ using different MLC schemes and Zhong's explicit schemes. The non-dimensional grid spacing $\beta$ is defined as,

$$\beta = k \cdot h \tag{41}$$

where $k$ is the wavenumber, and $h$ is the dimensional grid spacing. In Fig. 19 a), the errors of the original 1-1-1-1 scheme and 2-2-2-2 scheme grow abruptly during grid refinement when $\beta$ is too small. This deterioration of solution is the result of the minor numerical instability of the original MLC scheme presented in Section III.A. In the periodic simulation, there is no boundary source term to correct the numerical error, eventually, the simulation may diverge if any numerical instability exists. The Fourier analysis in Fig. 8, Fig. 10, and Fig. 12 show that the original 2-2-2-2 scheme has the largest magnitude of instability, then follows the 1-1-1-1 scheme and 2-2-1-1 scheme. It can explain why the error of the 2-2-2-2 scheme increases faster than that of the 1-1-1-1 scheme, and the 2-2-1-1 scheme is still stable in Fig. 19 a). As a comparison, the new MLC scheme is always stable during the grid refinement, and it also shows smaller error than the original MLC scheme with the same stencil. This observation further proves the increase of spectral resolution of the new MLC scheme due to the introduce of $u_{xy}$. In Fig. 19 b), Zhong's explicit schemes are compared with the new MLC scheme as well. All schemes are stable during the grid refinement; however, the error of the new MLC scheme is much smaller. The comparison verifies the main advantage of the MLC scheme over conventional finite difference methods – the spectral-like resolution.

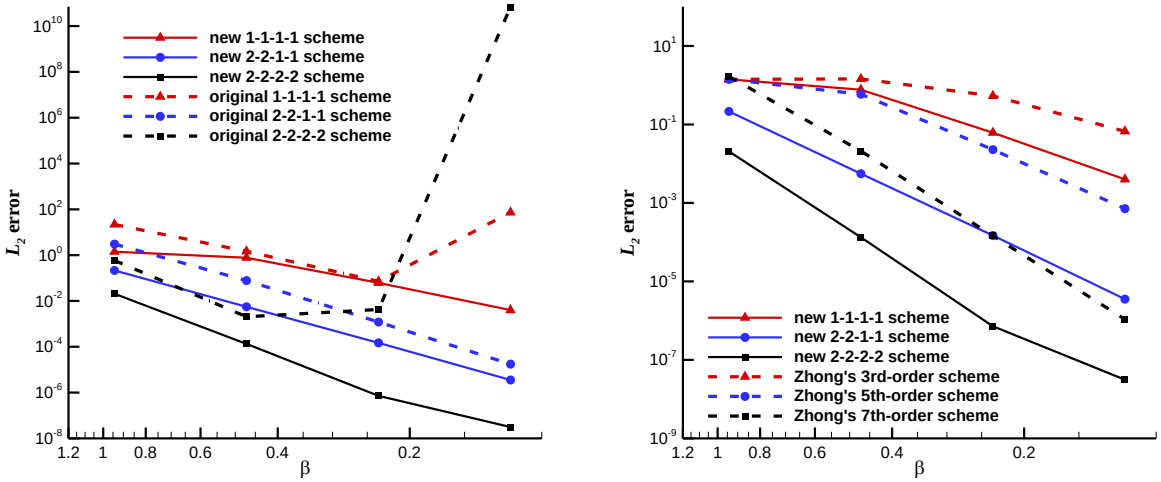


a) b)

**Fig. 19. Evolution of the $L_2$ error versus the non-dimensional grid spacing for 2-D linear advection with periodic boundary conditions ($t$ = 100).**

Table 6 compares the CPU time of several new MLC schemes with those of original MLC schemes which have the same stencils and order of accuracies. It demonstrates that the simulation with the new MLC scheme always runs faster, and the advantage of the new scheme becomes more significant when the order of accuracy increases. As explained in Section II.A, although the directional discretization technique introduces an additional equation to solve, it avoids the time-consuming approximation of cross derivatives. Overall, it leads to better computational efficiency, especially for high-order MLC schemes.

**Table 6. CPU time of the original and new MLC scheme for 2-D linear advection with periodic boundary conditions ($t$ = 100).**

| $N$ | 3rd-order 1-1-1-1 scheme, $\alpha$ = 1.5 | | 5th-order 2-2-1-1 scheme, $\alpha$ = -1 | | 7th-order 2-2-2-2 scheme, $\alpha$ = 12 | |
|---|---|---|---|---|---|---|
| | Original | New | Original | New | Original | New |
| 10 | 6.15E+00 | 4.59E+00 | 7.21E+00 | 5.30E+00 | 9.78E+00 | 5.95E+00 |
| 20 | 4.62E+01 | 3.56E+01 | 5.50E+01 | 3.96E+01 | 7.52E+01 | 4.56E+01 |
| 40 | 3.63E+02 | 2.76E+02 | 4.37E+02 | 3.09E+02 | 5.89E+02 | 3.42E+02 |
| 80 | 3.20E+03 | 2.76E+03 | 3.76E+03 | 2.99E+03 | 4.95E+03 | 3.35E+03 |
| 160 | 2.44E+04 | 2.26E+04 | 2.99E+04 | 2.45E+04 | 3.96E+04 | 2.77E+04 |

***Results of Non-Periodic Boundary Conditions***

In the next place, the results of non-periodic boundary conditions are analyzed. As described in Fig. 16, the inflow boundary conditions in Eq. (36) are enforced at the bottom and left boundaries; while the characteristic boundary conditions are applied to the top and right boundaries through the one-sided MLC schemes. The long-time simulation results at $t$ = 100 (212 wavelengths) are used to compare the accuracy and stability of the original and new MLC schemes.

Table 7 presents the errors and rates of convergence of the new 1-1-1-1 scheme and the original 1-1-1-1 scheme. The configuration of inner and boundary closure schemes follows Case 1 in Table 1 and Table 2. It demonstrates that both the new scheme and the original scheme can achieve or surpass the expected third-order global accuracy. Similar with the periodic simulation results, the original MLC scheme shows slightly higher rates of convergence because of the use of central scheme for cross derivatives. However, the difference is very small here because the lower order boundary closure schemes also affect the rates of convergence. On the other hand, the new 1-1-1-1 scheme still shows smaller error especially for small $N$'s due to its better spectral resolution. As suggested in Fig. 17, both the new and the original 1-1-1-1 scheme with the recommended $\alpha$ value of 1.5 are stable.

**Table 7. Errors and rates of convergence of the original and new 1-1-1-1 scheme (3rd order) for 2-D linear advection with non-periodic boundary conditions ($t$ = 100).**

| $N$ | Original 1-1-1-1 scheme, $\alpha$ = 1.5 | | | | New 1-1-1-1 scheme, $\alpha$ = 1.5 | | | |
|---|---|---|---|---|---|---|---|---|
| | $L_1$ error | Order | $L_2$ error | Order | $L_1$ error | Order | $L_2$ error | Order |
| 10 | 1.46E+00 | \ | 1.42E+00 | \ | 4.87E-01 | \ | 4.47E-01 | \ |
| 20 | 1.53E-01 | 3.25 | 1.36E-01 | 3.38 | 6.43E-02 | 2.92 | 5.73E-02 | 2.96 |
| 40 | 8.54E-03 | 4.17 | 7.47E-03 | 4.18 | 5.65E-03 | 3.51 | 4.95E-03 | 3.53 |
| 80 | 4.60E-04 | 4.21 | 4.04E-04 | 4.21 | 3.99E-04 | 3.82 | 3.51E-04 | 3.82 |
| 160 | 2.70E-05 | 4.09 | 2.38E-05 | 4.09 | 2.59E-05 | 3.94 | 2.28E-05 | 3.94 |

Similarly, Table 8 compares errors and rates of convergence from the original 2-2-2-2 scheme and the new 2-2-2-2 scheme. The configuration of inner and boundary closure schemes follows Case 2 in Table 1 and Table 2. The results demonstrate that the original 2-2-2-2 scheme with the recommended $\alpha$ value of 12 is unstable, as predicted by the matrix method in Fig. 18. It should be noted that the divergence is not merely caused by the minor numerical instability from the inner scheme, but the combined effect from the inner scheme and boundary closure schemes. If $\alpha$ is increased to 36, the original 2-2-2-2 scheme becomes stable but includes large dissipation. The results also demonstrate that the new 2-2-2-2 scheme with $\alpha$ value of 12 is stable, which suggests that the new MLC schemes should have better boundary stability in very high-order cases.

Similar with the comparison in Table 7, the original 2-2-2-2 scheme shows slightly higher rates of convergence than the new 2-2-2-2 scheme; however, the new scheme outperforms the original scheme in accuracy, as the error is much smaller on the same mesh. Therefore, the advantage of the new MLC scheme on accuracy is still significant in cases with non-periodic boundaries.

**Table 8. Errors and rates of convergence of the original and new 2-2-2-2 scheme (7th order) for 2-D linear advection with non-periodic boundary conditions ($t$ = 100).**

| $N$ | Original 2-2-2-2 scheme, $\alpha$ = 12 | | | | Original 2-2-2-2 scheme, $\alpha$ = 36 | | | | New 2-2-2-2 scheme, $\alpha$ = 12 | | | |
|---|---|---|---|---|---|---|---|---|---|---|---|---|
| | $L_1$ error | Order | $L_2$ error | Order | $L_1$ error | Order | $L_2$ error | Order | $L_1$ error | Order | $L_2$ error | Order |
| 10 | 1.18E+13 | \ | 1.22E+13 | \ | 1.84E+00 | \ | 1.80E+00 | \ | 2.92E-02 | \ | 2.26E-02 | \ |
| 20 | 6.42E+25 | \ | 5.79E+25 | \ | 7.63E-03 | 7.91 | 8.84E-03 | 7.67 | 2.05E-04 | 7.16 | 1.72E-04 | 7.04 |
| 40 | 2.09E+53 | \ | 1.79E+53 | \ | 2.79E-05 | 8.10 | 2.74E-05 | 8.33 | 1.27E-06 | 7.33 | 1.00E-06 | 7.42 |
| 80 | 1.88E+111 | \ | 1.66E+111 | \ | 9.44E-08 | 8.20 | 8.94E-08 | 8.26 | 6.26E-09 | 7.66 | 4.90E-09 | 7.68 |
| 160 | 8.90E+229 | \ | ∞ | \ | 4.30E-10 | 7.78 | 3.67E-10 | 7.93 | 2.13E-10 | 4.88 | 1.87E-10 | 4.71 |

In summary, the numerical tests on the two-dimensional linear advection equation demonstrates that the new MLC scheme has smaller errors in both cases with the periodic or non-periodic boundary conditions due to the additional degree of freedom $u_{xy}$; and the advantage is more significant for very high-order schemes. The long-time simulation result demonstrates that the new MLC scheme has better computational efficiency especially for the very high-order schemes, because the directional discretization in the new scheme avoids the cross-derivative approximation. The long-time simulation also verifies that the new MLC scheme is always stable for both periodic and non-periodic boundary conditions, while the original MLC scheme could be unstable in some cases. Specifically, the deterioration of the solution is observed in the original 1-1-1-1 and 2-2-2-2 scheme for periodic boundary conditions; the original 2-2-2-2 scheme with recommended $\alpha$ value of 12 is unstable for non-periodic boundary conditions.

### B. Nonlinear Euler Equations

To apply the MLC scheme on the Euler equations (1), the auxiliary equations are required. For the original MLC scheme, auxiliary equations for first derivatives of $U$ are introduced. In the spatial discretization, the locally

global Lax-Friedrichs approach is first applied on the inviscid flux terms; then, the upwind and downwind schemes can be used to discretize the positive flux and negative flux. The details of the methodology for the original MLC scheme is described in [1]. For the new MLC scheme, the procedures are very similar with those in [1]. The main difference is that there are additional auxiliary equations for the cross derivatives of $U$ to solve, therefore, the derivation and resulting formulas are more complicated. However, the numerical tests in this section can prove that the computational efficiency is improved due to the avoidance of the cross-derivative approximations for the flux terms. The procedures for applying the new MLC scheme on the Euler equations are briefly described in the following.

In the Cartesian coordinates ($x_1$, $x_2$, $x_3$), the auxiliary equations for first derivatives are introduced as follows,

$$\frac{\partial U_{x_k}}{\partial t} + \frac{\partial F_{jx_k}}{\partial x_j} = 0 \tag{42}$$

where $j$, $k$ = (1, 2, 3), and $j$ is a dummy index. Eq. (42) is the same auxiliary equations as used in the original MLC scheme. It has two or three components in two-dimensional or three-dimensional cases respectively. For the new MLC scheme, auxiliary equations for cross derivatives are derived by taking derivatives on Eq. (42). It should be mentioned that the formulation for three-dimensional cases are different with that for two-dimensional cases, which is not discussed in this paper. Accordingly, the description below only focuses on the two-dimensional case. The auxiliary equation for the cross derivative $U_{xy}$ in two-dimensional cases is of the form,

$$\frac{\partial U_{xy}}{\partial t} + \frac{\partial F_{1xy}}{\partial x} + \frac{\partial F_{2xy}}{\partial y} = 0 \tag{43}$$

The Euler equations (1) and the auxiliary equations (42) and (43) can be written in vector forms as follows,

$$\frac{\partial}{\partial t}\begin{bmatrix} U \\ U_x \\ U_y \\ U_{xy} \end{bmatrix} = -\begin{bmatrix} F_{1x} + F_{2y} \\ F_{1xx} + F_{2xy} \\ F_{1xy} + F_{2yy} \\ F_{1yxx} + F_{2xyy} \end{bmatrix} \tag{44}$$

Similar as Eq. (22), 3 additional degrees of freedom can be defined as,

$$V = U_x, \quad W = U_y, \quad R = U_{xy} \tag{45}$$

Since $F_1$ and $F_2$ are nonlinear functions of $U$, the Jacobian matrices $A_1 = \partial F_1/\partial U$ and $A_2 = \partial F_2/\partial U$ are introduced. Then, the first derivatives and the cross derivatives of inviscid fluxes in Eq. (44) can be computed analytically as follows,

$$\begin{aligned} &F_{1x} = A_1 V, \quad F_{1y} = A_1 W, \quad F_{1xy} = A_1 R + A_{1y} V \\ &F_{2x} = A_2 V, \quad F_{2y} = A_2 W, \quad F_{2xy} = A_2 R + A_{2x} W \end{aligned} \tag{46}$$

Combining Eqs. (44) - (46), the system of equations used for the new MLC scheme can be obtained,

$$\frac{\partial}{\partial t}\begin{bmatrix} U \\ V \\ W \\ R \end{bmatrix} = -\begin{bmatrix} A_1 V + A_2 W \\ F_{1xx} + A_2 R + A_{2x} W \\ A_1 R + A_{1y} V + F_{2yy} \\ F_{1yxx} + F_{2xyy} \end{bmatrix} \tag{47}$$

Because the fluxes and their derivatives are calculated from Eqs. (3) and (46), it is clear that $F_{1xx}$, $F_{1yxx}$ in Eq. (47) can be discretized along the $x$ direction, and $F_{2yy}$, $F_{2xyy}$ can be discretized along the $y$ direction. The discretization follows the same formula as given in Eqs. (23) and (24).

Before applying the upwind MLC schemes, the locally global Lax-Friedrichs approach [1] is used to the split the inviscid flux terms. All fluxes and their derivatives are decomposed into positive and negative wave fields as follows,

$$\begin{aligned} F_j &= F_j^+ + F_j^- \\ F_{jx_k} &= F_{jx_k}^+ + F_{jx_k}^- \\ F_{jx_kx_j} &= F_{jx_kx_j}^+ + F_{jx_kx_j}^- \\ F_{jx_kx_jx_j} &= F_{jx_kx_jx_j}^+ + F_{jx_kx_jx_j}^- \end{aligned} \tag{48}$$

where the subscripts $j$, $k$ = (1, 2). Note that $j$ is not dummy index any more in Eq. (48). The derivatives that need to be discretized in Eq. (47) are,

$$
\begin{aligned}
F_{jx_jx_j} &= F^+_{jx_jx_j} + F^-_{jx_jx_j} \\
F_{jx_kx_jx_j} &= F^+_{jx_kx_jx_j} + F^-_{jx_kx_jx_j}, \quad j,\ k = (1,\ 2),\ \text{and}\ j \neq k
\end{aligned}
\tag{49}
$$

The positive part in Eq. (49) is approximated by the upwind MLC scheme along the *j* direction, and the negative part is approximated by the downwind scheme in the same manner. The downwind MLC scheme has the same formula as the upwind scheme in Eqs. (23) and (24), but the opposite sign in $\alpha$. It is required that the flux $F_j^+$ and $F_j^-$ contains only positive and negative eigenvalues in their Jacobian matrices respectively. A straightforward approach to construct $F_j^+$ and $F_j^-$ and their first and cross derivatives are,

$$
F_j^+ = \frac{1}{2}(F_j + \Lambda U), \quad F_j^- = \frac{1}{2}(F_j - \Lambda U) \tag{50}
$$

where, $\Lambda$ is a positive parameter that is a constant within each stencil, but a variant for stencils at different base point. The first derivatives and cross derivatives in Eq. (46) can be decomposed in the same manner. Within an arbitrary stencil, $\Lambda$ is determined from,

$$
\Lambda = \max(\lambda_i) \tag{51}
$$

where $\lambda_i$ is a positive parameter chosen to be larger than the local maximum eigenvalues of the Jacobian $A_j$ on the grid point *i*. The procedure is repeated for every base point. Compared with using a constant $\lambda$ in the entire domain, the locally global Lax-Friedrichs approach has lower dissipation. After the MLC approximations, Eq. (47) becomes a system of ordinary differential equations, which can be solved by the Runge-Kutta methods.

The discretization described above is performed with respect to the Cartesian coordinates, and this is straightforward for rectangular physical domains. In general case, the physical domain can have different shapes where curvilinear meshes are required. Therefore, a coordinate transformation between physical and computational domain can be applied to the governing equations, and the discretization with the MLC schemes can be applied in the computational domain, which is very similar to the description above.

In the following part of this section, the two-dimensional Euler equations in the Cartesian coordinates are solved. A rectangular domain with periodic boundary conditions are used in all test cases. Because there is no physical boundary in the domain, uniform mesh in both directions is used, and no boundary closure schemes are required. In all the test cases, the new and original MLC scheme are compared, as well as Zhong's upwind explicit scheme. Meanwhile, a fourth-order Runge-Kutta method is applied for time integration. The CFL number is set to be 0.1 for short-time simulation, and 0.2 for long-time simulation. The small CFL number ensures stability and can maintain small error from time integration.

***Two-Dimensional Entropy Wave***

The first test case for the Euler equations is the two-dimensional entropy wave in (*x*, *y*) plane. The exact solution and initial condition (*t*=0) are given as follows,

$$
\begin{aligned}
\rho(x, y, t) &= 1 + 0.2\sin(\pi(x + y - (u + v)t)) \\
u(x, y, t) &= 0.7 \\
v(x, y, t) &= 0.3 \\
p(x, y, t) &= 1
\end{aligned}
\tag{52}
$$

To be general, there is an angle between the wave vector and mean flow velocity. The wave vector has an angle of $\pi/4$ from the *x*-axis, and the mean flow velocity has a smaller angle from the *x*-axis. The propagation of the two-dimensional entropy wave is a passive convection. For each location, only density and temperature change during the convection, while the density and temperature patterns from the initial condition are maintained.

The computational domain is a square field within the range of $0 < x < 2$ and $0 < y < 2$, which includes one wavelength in both *x* and *y*-direction. A uniform mesh with *N* grid panels in both dimensions is used, and periodic boundary conditions on all boundaries are applied.

Table 9 to Table 11 compare the errors and rates of convergence of the new MLC schemes, the original MLC schemes, and Zhong's upwind explicit schemes based on the solution of $\rho$ at $t = 2$ with CFL = 0.1. Each table shows the results from the schemes with the same order of accuracy. First, the results show that both the new and the original MLC schemes can surpass the expected order of accuracy by one except when the error is close to machine epsilon (see 2-2-2-2 schemes in Table 11), and the original scheme shows higher convergence rate due to the use of central schemes on cross derivatives, which is obvious in Table 10 and Table 11. Zhong's upwind explicit schemes can achieve their expected order as well. Second, the new MLC scheme shows smaller error than the original MLC scheme with the same order of accuracy; the advantage of the new scheme over the original scheme is more obvious in 5th- and 7th-order cases in Table 10 and Table 11 for small *N*, which is consistent with the observation in the

linear advection results. Besides, both the original and new MLC schemes are much more accurate than the corresponding Zhong's explicit scheme due to the spectral-like resolution.

**Table 9. Errors and rates of convergence of the new 1-1-1-1 scheme (3rd-order), the original 1-1-1-1 scheme (3rd-order), and Zhong's 3rd-order explicit scheme for 2-D entropy wave ($t$ = 2).**

| $N$ | Zhong's 3rd-order scheme, $\alpha$ = 0.25 | | Original 1-1-1-1 scheme, $\alpha$ = 1.5 | | New 1-1-1-1 scheme, $\alpha$ = 1.5 | |
|---|---|---|---|---|---|---|
| | $L_1$ error | Order | $L_1$ error | Order | $L_1$ error | Order |
| 5 | 6.37E-02 | \ | 1.41E-02 | \ | 1.16E-02 | \ |
| 10 | 7.29E-03 | 3.13 | 7.66E-04 | 4.20 | 7.12E-04 | 4.02 |
| 20 | 8.87E-04 | 3.04 | 4.47E-05 | 4.10 | 4.42E-05 | 4.01 |
| 40 | 1.08E-04 | 3.04 | 2.74E-06 | 4.03 | 2.73E-06 | 4.01 |
| 80 | 1.32E-05 | 3.03 | 1.70E-07 | 4.01 | 1.70E-07 | 4.01 |
| 160 | 1.64E-06 | 3.01 | 1.06E-08 | 4.00 | 1.06E-08 | 4.00 |

**Table 10. Errors and rates of convergence of the new 2-2-1-1 scheme (5th-order), the original 2-2-1-1 scheme (5th-order), and Zhong's 5th-order explicit scheme for 2-D entropy wave ($t$ = 2).**

| $N$ | Zhong's 5th-order scheme, $\alpha$ = -6 | | Original 2-2-1-1 scheme, $\alpha$ = -1 | | New 2-2-1-1 scheme, $\alpha$ = -1 | |
|---|---|---|---|---|---|---|
| | $L_1$ error | Order | $L_1$ error | Order | $L_1$ error | Order |
| 5 | 4.36E-02 | \ | 4.73E-03 | \ | 5.51E-04 | \ |
| 10 | 2.46E-03 | 4.15 | 7.55E-05 | 5.97 | 1.33E-05 | 5.38 |
| 20 | 1.20E-04 | 4.36 | 1.08E-06 | 6.13 | 2.83E-07 | 5.55 |
| 40 | 3.96E-06 | 4.91 | 1.27E-08 | 6.41 | 5.22E-09 | 5.76 |
| 80 | 1.23E-07 | 5.01 | 1.37E-10 | 6.53 | 8.73E-11 | 5.90 |
| 160 | 3.79E-09 | 5.02 | 1.68E-12 | 6.35 | 1.48E-12 | 5.88 |

**Table 11. Errors and rates of convergence of the new 2-2-2-2 scheme (7th-order), the original 2-2-2-2 scheme (7th-order), and Zhong's 7th-order explicit scheme for 2-D entropy wave ($t$ = 2).**

| $N$ | Zhong's 7th-order scheme, $\alpha$ = 36 | | Original 2-2-2-2 scheme, $\alpha$ = 12 | | New 2-2-2-2 scheme, $\alpha$ = 12 | |
|---|---|---|---|---|---|---|
| | $L_1$ error | Order | $L_1$ error | Order | $L_1$ error | Order |
| 5 | 8.62E-03 | \ | 8.13E-04 | \ | 9.43E-05 | \ |
| 10 | 3.91E-04 | 4.46 | 2.06E-06 | 8.63 | 4.16E-07 | 7.82 |
| 20 | 7.51E-06 | 5.70 | 4.76E-09 | 8.76 | 1.81E-09 | 7.85 |
| 40 | 7.09E-08 | 6.73 | 1.60E-11 | 8.21 | 1.29E-11 | 7.13 |
| 80 | 5.70E-10 | 6.96 | 4.33E-13 | 5.21 | 4.20E-13 | 4.94 |
| 160 | 4.43E-12 | 7.01 | 8.42E-14 | 2.36 | 8.54E-14 | 2.30 |

Similar with the analysis for the linear advection, the long-time simulation results with CFL = 0.2 at $t$ = 100, when the mean flow has traveled for 35 domain lengths in $x$ and 15 domain lengths in $y$, are presented to investigate the accuracy and stability of the MLC schemes. For the original MLC schemes, the deterioration of the solution is observed in the 2-2-1-1 scheme and the 2-2-2-2 scheme as shown in Fig. 20 a). Again, it is triggered by the minor numerical instability of the original MLC scheme because there is no boundary source term in the periodic simulation. As a comparison, the new MLC scheme is always stable during the grid refinement, and it also shows smaller error than the original MLC scheme on the 2-2-1-1 and 2-2-2-2 stencils. In Fig. 20 b), Zhong's explicit schemes are compared with the new MLC scheme as well. All schemes are stable during the grid refinement; however, the error of the new MLC scheme is much smaller. The long-time analysis proves that the stability and spectral resolution of the new MLC scheme is improved as well for the nonlinear Euler equations, compared with the original MLC scheme or Zhong's explicit scheme.

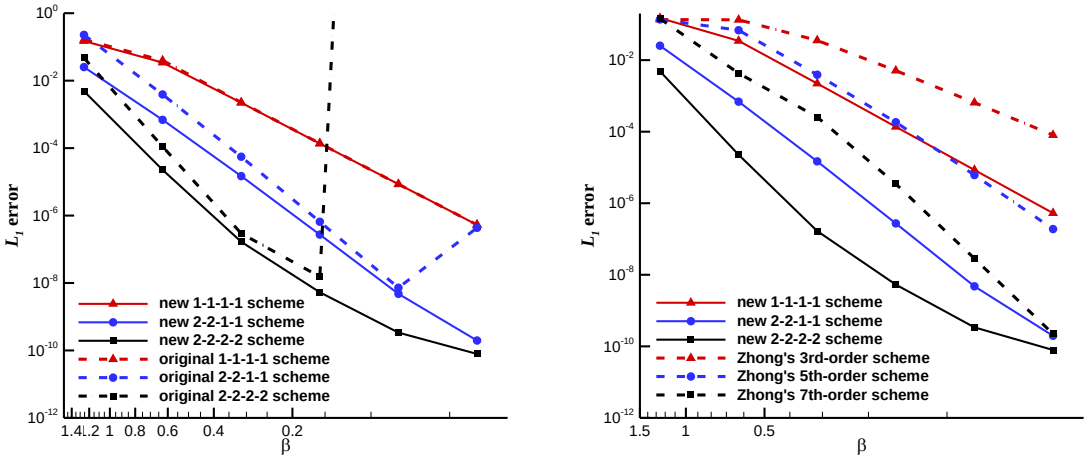


a) b)

**Fig. 20. Evolution of the $L_1$ error versus the non-dimensional grid spacing for 2-D entropy wave ($t$ = 100).**

Table 12 compares the CPU time of several new MLC schemes with those of original MLC schemes which have the same stencils and order of accuracies. Similar with what we observe for the linear advection equation, it shows that the simulation with the new MLC scheme also runs faster for the nonlinear Euler equation. The advantage of the new scheme becomes more significant when the order of accuracy increases, because the new MLC scheme avoids the approximation of cross derivatives, which is much more expensive than the second-derivative approximations for very high-order schemes. The comparison of CPU time here is more important than that in the linear advection, because most flow dynamic problems are governed by either the Euler equations or the Navier-Stokes equations. Therefore, it is a strong proof that the new MLC scheme can have better computational efficiency than the original MLC scheme in practical flow simulations.

**Table 12. CPU time of the original and new MLC scheme for 2-D entropy wave ($t$ = 100).**

| $N$ | 3rd-order 1-1-1-1 scheme, $\alpha$ = 1.5 | | 5th-order 2-2-1-1 scheme, $\alpha$ = -1 | | 7th-order 2-2-2-2 scheme, $\alpha$ = 12 | |
|---|---|---|---|---|---|---|
| | Original | New | Original | New | Original | New |
| 10 | 1.72E+00 | 1.39E+00 | 2.74E+00 | 1.60E+00 | 3.29E+00 | 1.65E+00 |
| 20 | 1.40E+01 | 1.04E+01 | 2.18E+01 | 1.17E+01 | 2.55E+01 | 1.22E+01 |
| 40 | 1.15E+02 | 8.56E+01 | 1.64E+02 | 9.54E+01 | 1.95E+02 | 1.02E+02 |
| 80 | 9.70E+02 | 7.11E+02 | 1.30E+03 | 7.95E+02 | 1.60E+03 | 8.38E+02 |
| 160 | 7.67E+03 | 5.90E+03 | 1.03E+04 | 6.56E+03 | 1.30E+04 | 7.24E+03 |

***Two-Dimensional Isentropic Vortex***

The second test case for the Euler equations is a two-dimensional inviscid isentropic vortex, which shows the performance of the current MLC schemes in vortical flow simulations. The vortex is superimposed to a uniform steady mean flow in the $x$-direction. The mean flow conditions are set as follows,

$$p_\infty = 101325[Pa],\quad T_\infty = 300[K],\quad M = 0.5$$
$$\rho_\infty = \frac{p_\infty}{RT_\infty},\qquad a_\infty = \sqrt{\gamma RT_\infty},\qquad U_\infty = Ma_\infty \tag{53}$$
$$\gamma = 1.4,\qquad R = 286.94\left[J\cdot kg^{-1}\cdot K^{-1}\right]$$

where $U_\infty$ is the mean velocity, and Mach number $M$ is set to be 0.5 in the following simulations. The initial conditions ($t$ = 0) involve the mean flow and a perturbation, which is an isentropic vortex defined as follows,

$$\delta u = -\sqrt{RT_\infty}\,\frac{\varepsilon}{2\pi}(y-y_0)e^{\varphi\left(1-r^2\right)},\quad \delta v = \sqrt{RT_\infty}\,\frac{\varepsilon}{2\pi}(x-x_0)e^{\varphi\left(1-r^2\right)},$$
$$\delta T = -T_\infty\frac{\varepsilon^2(\gamma-1)}{16\varphi\gamma\pi^2}e^{2\varphi\left(1-r^2\right)},\qquad \frac{\delta p}{p_\infty}+1=\left(\frac{\delta\rho}{\rho_\infty}+1\right)^{\gamma}=\left(\frac{\delta T}{T_\infty}+1\right)^{\gamma/\gamma-1} \tag{54}$$

where $(x_0, y_0)$ represents location of the vortex center, and $r^2 = (x-x_0)^2+(y-y_0)^2$. The constants $\varepsilon$ and $\varphi$ are factors related to the strength and width of the vortex. The perturbations in $(u, v)$ and $T$ are defined independently in Eq. (54), while $p$ and $\rho$ are determined by isentropic relations. In this paper, $\varepsilon$ = 1 and $\varphi$ = 1 are used. Therefore, the amplitude of perturbation in density $|\delta\rho/\rho_\infty|$ is about 6.27% at the vortex center. The vortex edge is defined at the

location where $|\delta\rho/\rho_\infty|$ = 0.1%, corresponding to $r$ = 1.15m. The exact solution of this problem is a passive convection of the perturbed mean flow, and the vortex maintains its structure during the convection. It is a good test case for assessing the ability of the MLC schemes with respect to vortex preservation, which is affected by the dissipation, dispersion, and anisotropic errors of the MLC schemes.

The computational domain is a square field within the range of $0 < x < L$ and $0 < y < L$, where $L$ = 22.0m. At $t$ = 0, the vortex core is located at the center of the domain. A uniform mesh with $N$ grid panels in both dimensions is used, and periodic boundary conditions are set on all boundaries. This domain is large enough to reduce the boundary effects because the initial perturbations on the computational boundaries are negligible.

Similar with the previous case of the two-dimensional entropy wave, a short-time simulation after the vortex has traveled approximate 10 diameters ($t$ = 0.1267s, CFL = 0.1) is first conducted to estimate the rate of convergence of the MLC schemes. The results based on the solution of $\rho$ from the new MLC schemes, the original MLC schemes, and Zhong's upwind explicit schemes are compared in Table 13 to Table 15. It should be noted that $N$ is relatively larger compared with other test cases because the computational domain is wider in this case. To be clear, the number of grid points within the vortex is given in the bracket. Similar with previous cases, the results demonstrate that all schemes can achieve the expected orders of accuracy. The new MLC scheme shows smaller error than the original MLC scheme with the same order of accuracy, and both the new and original MLC schemes are much more accurate than the corresponding Zhong's explicit scheme.

**Table 13. Errors and rates of convergence of the new 1-1-1-1 scheme, the original 1-1-1-1 scheme, and Zhong's 3rd-order explicit scheme for 2-D isentropic vortex after traveling 10*d*.**

| $N$ | Zhong's 3rd-order scheme, $\alpha$ = 0.25 | | Original 1-1-1-1 scheme, $\alpha$ = 1.5 | | New 1-1-1-1 scheme, $\alpha$ = 1.5 | |
|---|---|---|---|---|---|---|
| | $L_1$ error | Order | $L_1$ error | Order | $L_1$ error | Order |
| 20 (2) | 2.38E-03 | \ | 2.03E-03 | \ | 2.02E-03 | \ |
| 40 (4) | 1.67E-03 | 0.51 | 1.02E-03 | 1.00 | 8.66E-04 | 1.22 |
| 80 (8) | 6.26E-04 | 1.41 | 1.41E-04 | 2.86 | 1.14E-04 | 2.93 |
| 160 (16) | 1.17E-04 | 2.42 | 8.33E-06 | 4.08 | 7.29E-06 | 3.96 |
| 320 (32) | 1.56E-05 | 2.90 | 4.45E-07 | 4.23 | 4.14E-07 | 4.14 |

**Table 14. Errors and rates of convergence of the new 2-2-1-1 scheme, the original 2-2-1-1 scheme, and Zhong's 5th-order explicit scheme for 2-D isentropic vortex after traveling 10*d*.**

| $N$ | Zhong's 5th-order scheme, $\alpha$ = -6 | | Original 2-2-1-1 scheme, $\alpha$ = -1 | | New 2-2-1-1 scheme, $\alpha$ = -1 | |
|---|---|---|---|---|---|---|
| | $L_1$ error | Order | $L_1$ error | Order | $L_1$ error | Order |
| 20 (2) | 2.28E-03 | \ | 2.01E-03 | \ | 1.61E-03 | \ |
| 40 (4) | 1.34E-03 | 0.76 | 7.13E-04 | 1.49 | 1.18E-04 | 3.76 |
| 80 (8) | 2.81E-04 | 2.26 | 2.89E-05 | 4.63 | 6.17E-06 | 4.26 |
| 160 (16) | 2.63E-05 | 3.42 | 4.51E-07 | 6.00 | 1.75E-07 | 5.14 |
| 320 (32) | 1.34E-06 | 4.29 | 7.26E-09 | 5.95 | 3.69E-09 | 5.56 |

**Table 15. Errors and rates of convergence of the new 2-2-2-2 scheme, the original 2-2-2-2 scheme, and Zhong's 7th-order explicit scheme for 2-D isentropic vortex after traveling 10*d*.**

| $N$ | Zhong's 7th-order scheme, $\alpha$ = 36 | | Original 2-2-2-2 scheme, $\alpha$ = 12 | | New 2-2-2-2 scheme, $\alpha$ = 12 | |
|---|---|---|---|---|---|---|
| | $L_1$ error | Order | $L_1$ error | Order | $L_1$ error | Order |
| 20 (2) | 2.08E-03 | \ | 1.79E-03 | \ | 1.32E-03 | \ |
| 40 (4) | 8.86E-04 | 1.23 | 1.01E-04 | 4.14 | 1.15E-04 | 3.53 |
| 80 (8) | 7.25E-05 | 3.61 | 4.00E-06 | 4.66 | 2.50E-06 | 5.52 |
| 160 (16) | 2.98E-06 | 4.61 | 1.51E-08 | 8.05 | 1.02E-08 | 7.93 |
| 320 (32) | 2.84E-08 | 6.71 | 4.56E-11 | 8.37 | 3.05E-11 | 8.39 |

A long-time simulation is carried out in the next place. Specifically, the solution at $t$ = 1.267s (CFL = 0.2) is evaluated when the vortex has traveled approximate 100 diameters or 10 domain lengths in the $x$ direction. To investigate the anisotropic errors, Fig. 21 compares the density contours from the new 2-2-1-1 scheme, the original 2-2-1-1 scheme, and Zhong's fifth-order explicit scheme. All schemes have the same order of accuracy. Comparing Fig. 21 a), b), and c) which share the same mesh, we can observe that the new 2-2-1-1 scheme with the directional discretization has obvious advantage over the other two schemes in terms of maintaining the vortex structure. It generates isotropic density distribution after the long-time simulation. As a comparison, the vortex from the original 2-2-1-1 scheme has elliptic shape, which is the reflection of anisotropy. The vortex from Zhong's fifth-order explicit scheme with $N$ = 80 has almost damped out after the long-time simulation, which is due to larger dissipation. When the grid is refined as in Fig. 21 d), Zhong's fifth-order scheme also shows an anisotropic distribution in the density contours.

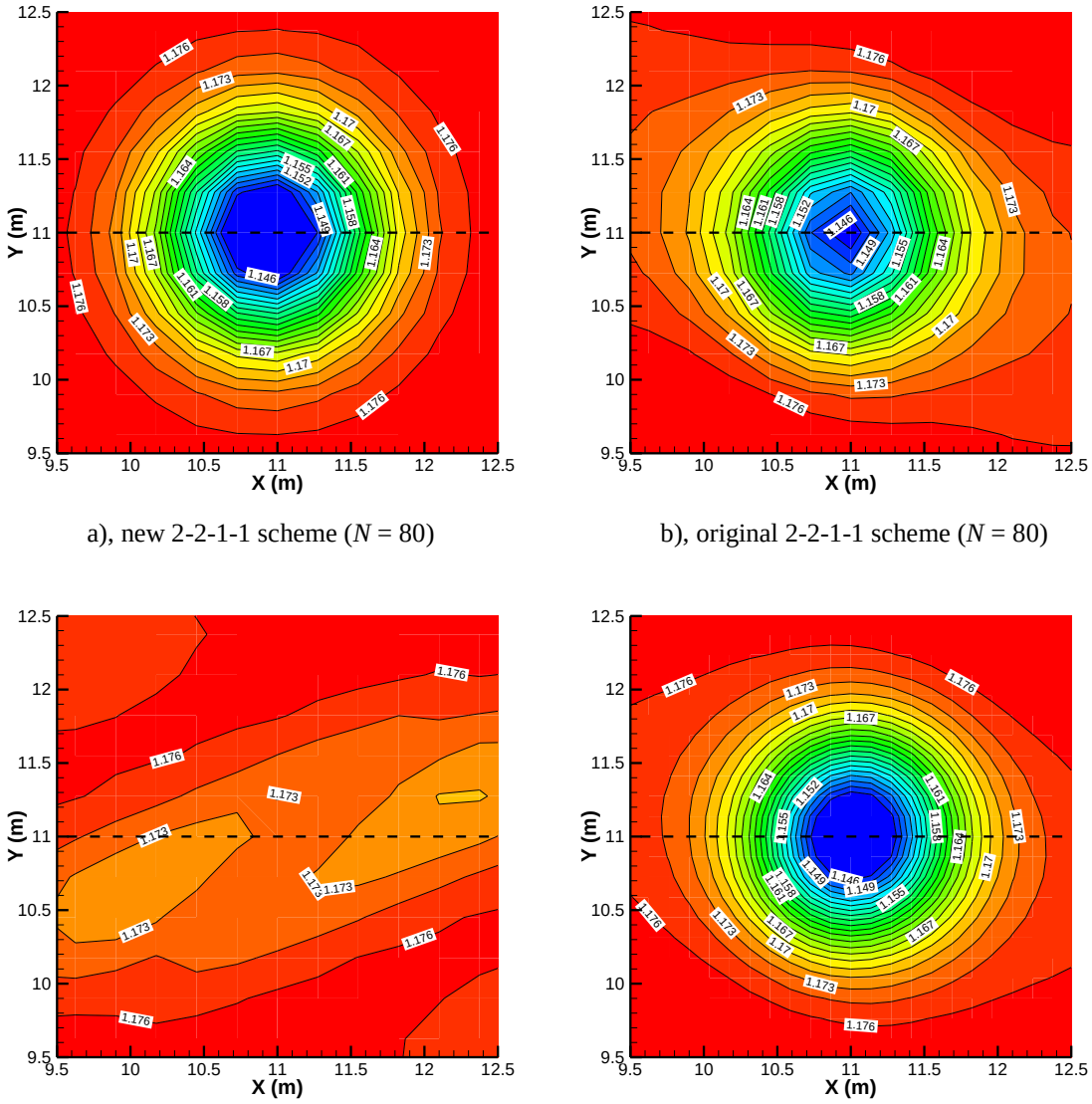


a), new 2-2-1-1 scheme ($N$ = 80)

b), original 2-2-1-1 scheme ($N$ = 80)

c), Zhong's 5th-order scheme ($N$ = 80)

d), Zhong's 5th-order scheme ($N$ = 160)

**Fig. 21. Comparison of density contours for 2-D isentropic vortex after traveling 100*d*.**

Fig. 22 presents the vorticity distribution along the centerline ($y$ = 11m) of the vortex, which is the black dashed line in Fig. 21. The fifth-order schemes are used for comparison and different mesh size are analyzed. All figures show clearly that the dissipative error decreases when the grid resolution increases. The dispersive error is not significant in these fifth-order schemes; while for lower-order scheme like the original 1-1-1-1 scheme, dispersive error may be observed [1]. Same as the anisotropic error, Fig. 22 shows the new 2-2-1-1 scheme has much smaller dissipation than the original 2-2-1-1 scheme when $N$ is 80, which is the result of the improved spectral resolution. When $N$ is increased to 160, both the new and the original 2-2-1-1 schemes are very accurate; however, Zhong's fifth-order explicit scheme still shows observable dissipation.

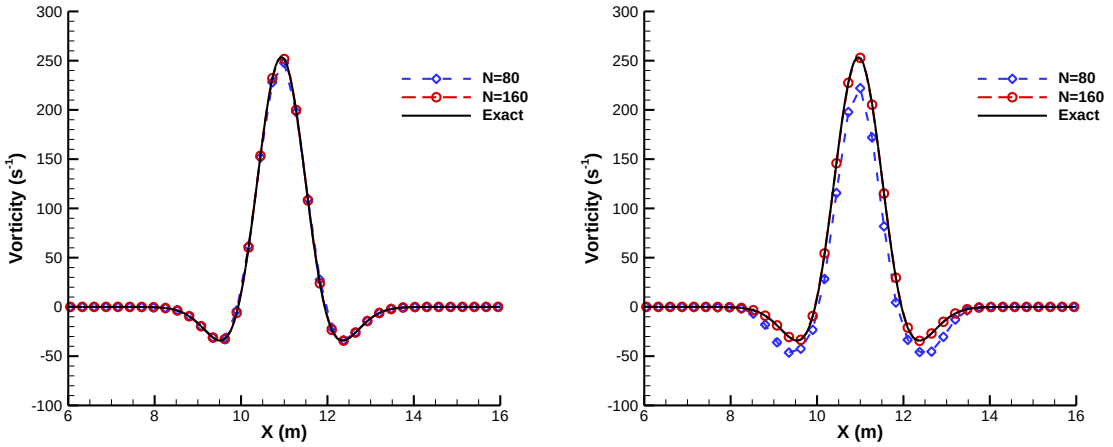


a), new 2-2-1-1 scheme

b), original 2-2-1-1 scheme

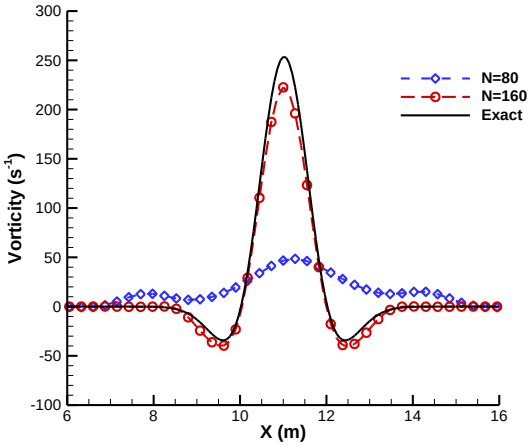


c), Zhong's 5th-order scheme

**Fig. 22. Comparison of vorticity distribution on the centerline in the *x*-direction for 2-D isentropic vortex after traveling 100*d*.**

For the sake of brevity, same analysis for third-order schemes or seven-order schemes is not presented in this paper. Similar conclusions as for fifth-order schemes can be obtained in those analysis.

In previous test cases of the linear advection and the entropy wave, the deterioration or divergence of the result is observed for the original MLC scheme in long-time simulations. Although the case of the isentropic vortex is quite stable compared with other cases, it turns out the original MLC scheme can also diverge in very high-order cases if the simulation is kept running. Table 16 shows the numerical results at $t$ = 6.337s (CFL = 0.2), when the vortex has traveled approximate 500 diameters or 50 domain lengths in the $x$ direction. The new and original 2-2-2-2 schemes with seventh-order of accuracy are compared. It demonstrates that on the same mesh configuration, the new 2-2-2-2 scheme has smaller error. Moreover, the original 2-2-2-2 scheme shows deteriorated results when $N$ is increased to 160, which means the refined mesh generates less accurate results. When $N$ is increased to 320, the result with the original 2-2-2-2 scheme diverges. This is due to the minor numerical instability of the original MLC scheme. On the other hand, the new MLC scheme is always stable and the error decreases during the refinement of the mesh.

**Table 16. Errors and rates of convergence of the original and new 2-2-2-2 scheme (7th order) after the vortex traveling for 500 diameters.**

| $N$ | Original 2-2-2-2 scheme, $\alpha$ = 12 | | New 2-2-2-2 scheme, $\alpha$ = 12 | |
|---|---|---|---|---|
| | $L_1$ error | $L_\infty$ error | $L_1$ error | $L_\infty$ error |
| 20 (2) | 2.63E-03 | 2.50E-03 | 2.42E-03 | 2.40E-03 |
| 40 (4) | 2.80E-03 | 2.22E-03 | 2.40E-03 | 2.21E-03 |

| | | | | |
|---|---|---|---|---|
| 80 (8) | 4.09E-04 | 4.20E-04 | 2.17E-04 | 2.21E-04 |
| 160 (16) | 1.34E-03 | 1.48E-03 | 6.65E-05 | 6.64E-05 |
| 320 (32) | ∞ | ∞ | 1.18E-05 | 1.20E-05 |

Fig. 23 presents the density contours for original and new 2-2-2-2 schemes. It shows clearly that original 2-2-2-2 scheme generates deteriorated results during the mesh refinement; while for the new scheme, the anisotropic error is reduced when $N$ is increased from 80 to 160.

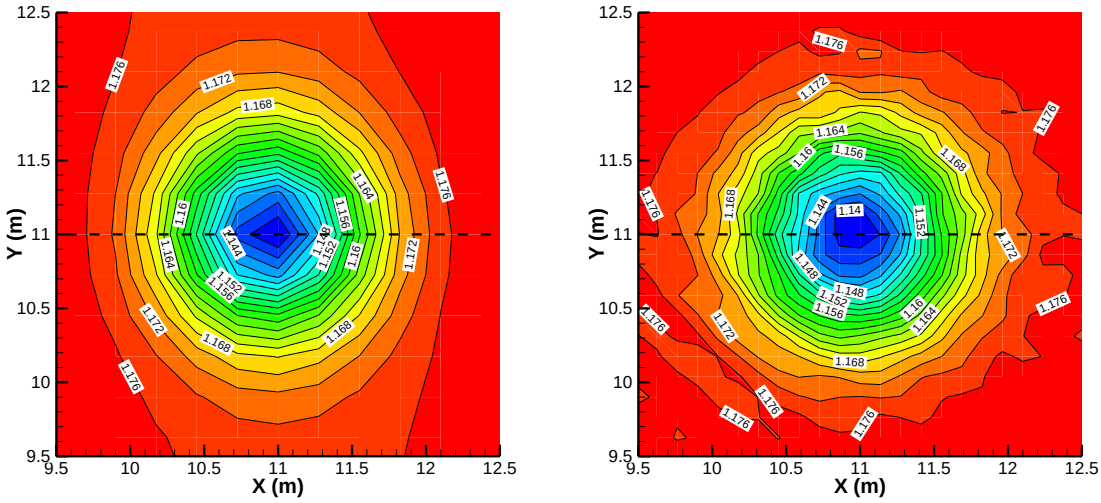


a), original 2-2-2-2 scheme ($N$ = 80)

b), original 2-2-2-2 scheme ($N$ = 160)

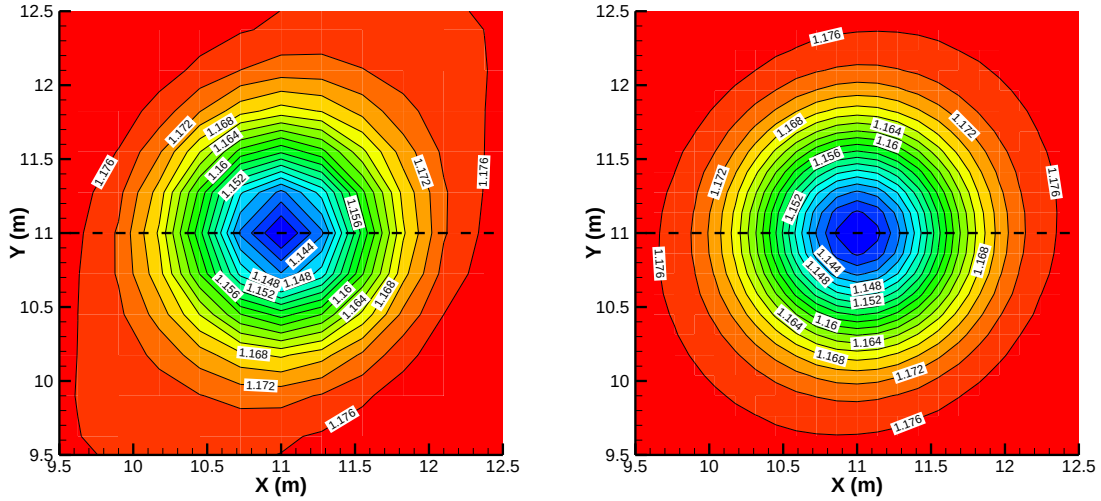


c), new 2-2-2-2 scheme ($N$ = 80)

d), new 2-2-2-2 scheme ($N$ = 160)

**Fig. 23. Comparison of density contours for 2-D isentropic vortex after traveling 500*d*.**

In summary, the numerical tests on the two-dimensional Euler equations demonstrates that the new MLC scheme has smaller errors in both the entropy wave and isentropic vortex simulations due to the additional degree of freedom $u_{xy}$; and the advantage is more significant for very high-order schemes. The analysis on long-time simulation results proves that the computational efficiency of the new MLC scheme, especially in the very high-order cases, is improved for the nonlinear Euler equations, which is of more significance for practical flow problems. The long-time simulation also verifies that the new MLC scheme is always stable in both the entropy wave and isentropic vortex cases, while the original MLC scheme could be unstable when the simulation is kept running. Specifically, the deterioration of the solution is observed in the original 2-2-1-1 scheme in the entropy wave; and the original 2-2-2-2 scheme diverges in both the entropy wave and isentropic vortex simulations. The isentropic vortex also shows that the new MLC scheme with the directional discretization has advantage over the original MLC

scheme or Zhong's explicit scheme in terms of maintaining the vortex structure, which benefits from the smaller anisotropic error and dissipation.

Chapter 4 tests the performance of the new MLC scheme with the two-dimensional linear advection equation and the two-dimensional nonlinear Euler equations. The original MLC scheme and Zhong's upwind explicit scheme are used for comparison. All numerical results demonstrate that the new MLC scheme has smaller errors than the original MLC scheme with the same order of accuracy, due to the better spectral resolution; and both the new and original MLC schemes are much more accurate than the corresponding Zhong's upwind explicit scheme. With the directional discretization, the new MLC scheme has better computational efficiency than the original scheme in both the linear advection equation and the Euler equations. The new MLC scheme also overcomes the minor numerical instability of the original MLC scheme; while the original MLC scheme may show deteriorated or diverged solution in very long-time simulations. It needs to be mentioned that periodic boundary conditions are used in all the diverged results, where there is no boundary source term to correct the error. In flow simulations with physical boundaries, the numerical instability of the original MLC scheme can be suppressed.

## V. Discussions and Conclusions

In this paper, the very high-order upwind multi-layer compact (MLC) scheme developed by Bai and Zhong [1] is revisited and analyzed with focus on the two-dimensional case. The goal is to resolve some remaining problems in the original MLC scheme [1] for two-dimensional simulations. Specifically, we want to overcome the minor numerical instability triggered by the inconsistency between the 1-D and 2-D MLC formulations, remove the uncertainty in cross-derivative approximation, and improve the accuracy and computational efficiency of the original MLC scheme. In the new MLC scheme presented here, a directional discretization technique is designed to extend the 1-D upwind scheme to two-dimensional cases. By introducing the auxiliary equation for the cross derivative, the spatial discretization can be fulfilled along each dimension independently. This directional discretization technique avoids any inconsistency from the 1-D and 2-D MLC formulations, such as the difference between the 1-D upwind scheme and the 2-D central scheme. It also overcomes the uncertainty arising from the approximation of cross derivatives. The two-dimensional Fourier analysis is performed to investigate the stability, accuracy, and spectral resolution of the new MLC schemes; and the matrix method is used to analyze the stability of the boundary closure schemes. Various flow problems governed by the linear advection equation, and the nonlinear Euler equations are simulated with the new MLC scheme. The results are compared with the analytical solutions and numerical solutions from the original MLC scheme and Zhong's upwind explicit scheme. The main conclusions are listed below.

1) The Fourier analysis demonstrates that the new MLC scheme is always stable in two-dimensional cases; while the original MLC scheme shows minor numerical instabilities when both the convention angle and Fourier wave angle is non-zero. The new MLC scheme also has better spectral resolution than the original MLC scheme for two-dimensional cases, due to its additional degree of freedom – the cross derivative.

2) The anisotropy analysis of the phase speed shows that the new MLC scheme has smaller dispersive error than the original MLC scheme along any orientation, and the anisotropic error is also reduced for a large portion of wavenumbers in $[0, 2\pi]$.

3) The analysis with the matrix methods indicates that stable boundary closure schemes are also easier to be obtained for the new MLC scheme in two-dimensional cases. The new MLC scheme shows much better boundary stability for small $\alpha$ values; while the original MLC scheme, specifically the seventh-order 2-2-2-2 scheme, requires very large $\alpha$ values which introduce too much dissipation.

4) The numerical tests on the linear advection equation, and the Euler equations demonstrate that the new MLC scheme can achieve smaller errors compared with the original MLC schemes or Zhong's explicit schemes, due to the additional degree of freedom – the cross derivative. Specifically, the isentropic vortex case shows that the new MLC scheme has significant advantage in terms of maintaining the vortex structure, which benefits from the smaller anisotropy and dissipation. By avoiding the time-consuming cross-derivative approximation, the new MLC scheme also has better computational efficiency. Both the advantage on accuracy and computational efficiency of the new MLC scheme is more significant in very high-order schemes, which is desirable for complex flow problems that requires extremely accurate numerical methods.

5) The long-time simulation verifies that the original MLC scheme could be unstable in some cases. Specifically, the deterioration of the solution is observed in the original 1-1-1-1 and 2-2-2-2 scheme in the linear advection with periodic boundary conditions; the original 2-2-2-2 scheme with recommended $\alpha$ value of 12 is unstable for the linear advection with non-periodic boundary conditions; and the deterioration of the solution is observed in the original 2-2-1-1 and 2-2-2-2 scheme in Euler equations. On the other hand, the new MLC schemes

with various orders of accuracy are always stable for both periodic and non-periodic boundary conditions, which is consistent with the Fourier analysis and boundary stability analysis.

It can be concluded that the new MLC scheme with the directional discretization overcomes the minor numerical instability and the uncertainty in the original MLC scheme; and the new MLC scheme also shows improved accuracy and computational efficiency in two-dimensional simulations. Future work will include its application to the Navier-Stokes simulations, and the extension to the three-dimensional case.

## Appendix

The 2-D boundary closures scheme used in Table 1 for cross derivatives are presented in this appendix. For Case 1, only two boundary closure schemes at ($i = N$, $j = 1$ to $N$-1) and ($i = N$, $j = N$) are needed; For Case 2, five boundary closure schemes at ($i = N$-1, $j = 2$ to $N$-2), ($i = N$, $j = 2$ to $N$-2), ($i = N$-1, $j = N$-1), ($i = N$, $j = N$-1), ($i = N$, $j = N$) are needed. For other grid points, the scheme formulas can be easily derived from symmetry.

### A. Boundary Closure Schemes in Case 1

***i = N, j = 1 to N-1 (3rd-order scheme)***

$$\begin{aligned}\left(u_{xy}\right)_{i,j} = {} & \frac{1}{h^2}\left(-\frac{1}{2}u_{i-1,j-1}+\frac{1}{2}u_{i,j-1}+\frac{1}{2}u_{i-1,j+1}-\frac{1}{2}u_{i,j+1}\right) \\ & +\frac{1}{h}\left(-\frac{1}{2}\left(u_x\right)_{i,j-1}+\frac{1}{2}\left(u_x\right)_{i,j+1}\right)+\frac{1}{h}\left(-\left(u_y\right)_{i-1,j}+\left(u_y\right)_{i,j}\right)\end{aligned} \tag{55}$$

***i = N, j = N (2nd-order scheme)***

$$\begin{aligned}\left(u_{xy}\right)_{i,j} = {} & \frac{1}{h^2}\left(-u_{i-1,j-1}+u_{i,j-1}+u_{i-1,j}-u_{i,j}\right) \\ & +\frac{1}{h}\left(-\left(u_x\right)_{i,j-1}+\left(u_x\right)_{i,j}\right)+\frac{1}{h}\left(-\left(u_y\right)_{i-1,j}+\left(u_y\right)_{i,j}\right)\end{aligned} \tag{56}$$

### B. Boundary Closure Schemes in Case 2

***i = N-1, j = 2 to N-2 (6th-order scheme)***

$$\begin{aligned}\left(u_{xy}\right)_{i,j} = {} & \frac{1}{h^2}\left(\frac{1}{24}u_{i-1,j-2}-\frac{1}{24}u_{i+1,j-2}-\frac{1}{3}u_{i-1,j-1}+\frac{1}{3}u_{i+1,j-1}+\frac{1}{3}u_{i-1,j+1}-\frac{1}{3}u_{i+1,j+1}-\frac{1}{24}u_{i-1,j+2}+\frac{1}{24}u_{i+1,j+2}\right) \\ & +\frac{1}{h}\left(\frac{1}{12}\left(u_x\right)_{i,j-2}-\frac{2}{3}\left(u_x\right)_{i,j-1}+\frac{2}{3}\left(u_x\right)_{i,j+1}-\frac{1}{12}\left(u_x\right)_{i,j+2}\right)+\frac{1}{h}\left(-\frac{1}{2}\left(u_y\right)_{i-1,j}+\frac{1}{2}\left(u_y\right)_{i+1,j}\right)\end{aligned} \tag{57}$$

***i = N, j = 2 to N-2 (6th-order scheme)***

$$\begin{aligned}\left(u_{xy}\right)_{i,j} = {} & \frac{1}{h^2}\begin{pmatrix}-\frac{1}{24}u_{i-2,j-2}+\frac{1}{6}u_{i-1,j-2}-\frac{1}{8}u_{i,j-2}+\frac{1}{3}u_{i-2,j-1}-\frac{4}{3}u_{i-1,j-1}+u_{i,j-1} \\ -\frac{1}{3}u_{i-2,j+1}+\frac{4}{3}u_{i-1,j+1}-u_{i,j+1}+\frac{1}{24}u_{i-2,j+2}-\frac{1}{6}u_{i-1,j+2}+\frac{1}{8}u_{i,j+2}\end{pmatrix} \\ & +\frac{1}{h}\left(\frac{1}{12}\left(u_x\right)_{i,j-2}-\frac{2}{3}\left(u_x\right)_{i,j-1}+\frac{2}{3}\left(u_x\right)_{i,j+1}-\frac{1}{12}\left(u_x\right)_{i,j+2}\right)+\frac{1}{h}\left(\frac{1}{2}\left(u_y\right)_{i-2,j}-2\left(u_y\right)_{i-1,j}+\frac{3}{2}\left(u_y\right)_{i,j}\right)\end{aligned} \tag{58}$$

***i = N-1, j = N-1 (6th-order scheme)***

$$\begin{aligned}\left(u_{xy}\right)_{i,j} = {} & \frac{1}{h^2}\left(\frac{25}{108}u_{i-2,j-2}-\frac{25}{108}u_{i,j-2}+2u_{i-1,j-1}-2u_{i,j-1}-\frac{25}{108}u_{i-2,j}-2u_{i-1,j}+\frac{11}{8}u_{i,j}-\frac{14}{27}u_{i+1,j}-\frac{14}{27}u_{i,j+1}+\frac{14}{27}u_{i+1,j+1}\right) \\ & +\frac{1}{h}\left(\frac{1}{18}\left(u_x\right)_{i-2,j-2}+\left(u_x\right)_{i-1,j-1}-\frac{1}{18}\left(u_x\right)_{i-2,j}-\left(u_x\right)_{i-1,j}+\frac{1}{9}\left(u_x\right)_{i+1,j}-\frac{1}{9}\left(u_x\right)_{i+1,j+1}\right) \\ & +\frac{1}{h}\left(\frac{1}{18}\left(u_y\right)_{i-2,j-2}-\frac{1}{18}\left(u_y\right)_{i,j-2}+\left(u_y\right)_{i-1,j-1}-\left(u_y\right)_{i,j-1}+\frac{1}{9}\left(u_y\right)_{i,j+1}-\frac{1}{9}\left(u_y\right)_{i+1,j+1}\right)\end{aligned} \tag{59}$$

***i = N, j = N-1 (6th-order scheme)***

$$
\begin{aligned}
\left(u_{xy}\right)_{i,j} = \frac{1}{h^2}\left(\begin{array}{l}
\frac{1}{24}u_{i-3,j-3} - \frac{3}{16}u_{i-2,j-3} + \frac{3}{8}u_{i-1,j-3} - \frac{11}{48}u_{i,j-3} - \frac{1}{9}u_{i-3,j-2} + \frac{1}{2}u_{i-2,j-2} - u_{i-1,j-2} + \frac{11}{18}u_{i,j-2} \\
-\frac{1}{12}u_{i-3,j-1} + \frac{3}{8}u_{i-2,j-1} - \frac{3}{4}u_{i-1,j-1} + \frac{11}{24}u_{i,j-1} + \frac{11}{72}u_{i-3,j+1} - \frac{11}{16}u_{i-2,j+1} + \frac{11}{8}u_{i-1,j+1} - \frac{121}{144}u_{i,j+1}
\end{array}\right) \\
+\frac{1}{h}\left(\frac{1}{8}\left(u_x\right)_{i,j-3} - \frac{1}{3}\left(u_x\right)_{i,j-2} - \frac{1}{4}\left(u_x\right)_{i,j-1} + \frac{11}{24}\left(u_x\right)_{i,j+1}\right) \\
+\frac{1}{h}\left(-\frac{1}{3}\left(u_y\right)_{i-3,j} + \frac{3}{2}\left(u_y\right)_{i-2,j} - 3\left(u_y\right)_{i-1,j} + \frac{11}{6}\left(u_y\right)_{i,j}\right)
\end{aligned}
\tag{60}
$$

***i = N, j = N (6th-order scheme)***

$$
\begin{aligned}
\left(u_{xy}\right)_{i,j} = \frac{1}{h^2}\left(\frac{4}{3}u_{i-3,j-3} - \frac{4}{3}u_{i,j-3} + \frac{27}{4}u_{i-2,j-2} - \frac{27}{4}u_{i,j-2} - \frac{4}{3}u_{i-3,j} - \frac{27}{4}u_{i-2,j} + \frac{97}{12}u_{i,j}\right) \\
+\frac{1}{h}\left(\frac{1}{3}\left(u_x\right)_{i-3,j-3} + \frac{9}{2}\left(u_x\right)_{i-2,j-2} + 9\left(u_x\right)_{i-1,j-1} - \frac{1}{3}\left(u_x\right)_{i-3,j} - \frac{9}{2}\left(u_x\right)_{i-2,j} - 9\left(u_x\right)_{i-1,j}\right) \\
+\frac{1}{h}\left(\frac{1}{3}\left(u_y\right)_{i-3,j-3} - \frac{1}{3}\left(u_y\right)_{i,j-3} + \frac{9}{2}\left(u_y\right)_{i-2,j-2} - \frac{9}{2}\left(u_y\right)_{i,j-2} + 9\left(u_y\right)_{i-1,j-1} - 9\left(u_y\right)_{i,j-1}\right)
\end{aligned}
\tag{61}
$$

## Acknowledgments

This research was sponsored by the Air Force Office of Scientific Research, USAF, under AFOSR Grants #FA9550-15-1-0268, monitored by Dr. Ivett Leyva. The research was also supported by Office of Naval Research (ONR) Grant #N00014-17-1-2343, monitored by Dr. Knox Millsaps previously and by Dr. Eric Marineau presently. The computations are mainly run on XSEDE resources provided by TACC under grant number TG-ASC090076 supported by National Science Foundation. The first author Zeyu Bai would like to acknowledge the financial support from the China Scholarship Council. The views and conclusions contained herein are those of the authors and should not be interpreted as necessarily representing the official policies or endorsements either expressed or implied, of the Air Force Office of Scientific Research or the U.S. Government.

## References

1 Bai, Z., and Zhong, X., "New Very High-Order Upwind Multilayer Compact Schemes with Spectral-Like Resolution for Flow Simulations," *55th AIAA Aerospace Sciences Meeting*, Grapevine, Texas: American Institute of Aeronautics and Astronautics, 2017, pp. 1–42.

2 Dubiner, M., "Spectral Methods on Triangles and Other Domains," *Journal of Scientific Computing*, vol. 6, Dec. 1991, pp. 345–390.

3 Moser, R. D., Moin, P., and Leonard, A., "A Spectral Numerical Method for the Navier-Stokes Equations with Applications to Taylor-Couette Flow," *Journal of Computational Physics*, vol. 52, Dec. 1983, pp. 524–544.

4 Hussaini, M. Y., and Zang, T. A., "Spectral Methods in Fluid Dynamics," *Annual Review of Fluid Mechanics*, vol. 19, Jan. 1987, pp. 339–367.

5 Lele, S. K., "Compact Finite Difference Schemes with Spectral-like Resolution," *Journal of Computational Physics*, vol. 103, Nov. 1992, pp. 16–42.

6 Haras, Z., and Ta'asan, S., "Finite difference schemes for long-time integration," *Journal of Computational Physics*, vol. 114, Oct. 1994, pp. 265–279.

7 Ashcroft, G., and Zhang, X., "Optimized prefactored compact schemes," *Journal of Computational Physics*, vol. 190, Sep. 2003, pp. 459–477.

8 Hixon, R., "Prefactored Small-Stencil Compact Schemes," *Journal of Computational Physics*, vol. 165, Dec. 2000, pp. 522–541.

9 Kim, J. W., and Lee, D. J., "Optimized Compact Finite Difference Schemes with Maximum Resolution," *AIAA Journal*, vol. 34, May 1996, pp. 887–893.

10 Mahesh, K., "A Family of High Order Finite Difference Schemes with Good Spectral Resolution," *Journal of Computational Physics*, vol. 145, Sep. 1998, pp. 332–358.

11 Shukla, R. K., Tatineni, M., and Zhong, X., "Very high-order compact finite difference schemes on non-uniform grids for incompressible Navier–Stokes equations," *Journal of Computational Physics*, vol. 224, Jun. 2007, pp. 1064–1094.

12 Chu, P. C., and Fan, C., "A Three-Point Sixth-Order Nonuniform Combined Compact Difference Scheme," *Journal of Computational Physics*, vol. 148, Jan. 1999, pp. 663–674.

13 Cockburn, B., Lin, S.-Y., and Shu, C.-W., "TVB Runge-Kutta Local Projection Discontinuous Galerkin Finite Element

Method for Conservation Laws III: One-Dimensional Systems," *Journal of Computational Physics*, vol. 84, Sep. 1989, pp. 90–113.

[14] Cockburn, B., and Shu, C.-W., "The Runge–Kutta Discontinuous Galerkin Method for Conservation Laws V: Multidimensional Systems," *Journal of Computational Physics*, vol. 141, Apr. 1998, pp. 199–224.

[15] Qiu, J., Dumbser, M., and Shu, C.-W., "The discontinuous Galerkin method with Lax–Wendroff type time discretizations," *Computer Methods in Applied Mechanics and Engineering*, vol. 194, Oct. 2005, pp. 4528–4543.

[16] Zhu, J., Zhong, X., Shu, C.-W., and Qiu, J., "Runge–Kutta discontinuous Galerkin method using a new type of WENO limiters on unstructured meshes," *Journal of Computational Physics*, vol. 248, Sep. 2013, pp. 200–220.

[17] Yee, H. C., Sandham, N. D., and Djomehri, M. J., "Low-Dissipative High-Order Shock-Capturing Methods Using Characteristic-Based Filters," *Journal of Computational Physics*, vol. 150, Mar. 1999, pp. 199–238.

[18] Harten, A., "High resolution schemes for hyperbolic conservation laws," *Journal of Computational Physics*, vol. 49, Mar. 1983, pp. 357–393.

[19] Harten, A., Engquist, B., Osher, S., and Chakravarthy, S. R., "Uniformly high order accurate essentially non-oscillatory schemes, III," *Journal of Computational Physics*, vol. 71, Aug. 1987, pp. 231–303.

[20] Liu, X.-D., Osher, S., and Chan, T., "Weighted Essentially Non-oscillatory Schemes," *Journal of Computational Physics*, vol. 115, Nov. 1994, pp. 200–212.

[21] Jiang, G.-S., and Shu, C.-W., "Efficient Implementation of Weighted ENO Schemes," *Journal of Computational Physics*, vol. 126, Jun. 1996, pp. 202–228.

[22] Ekaterinaris, J. A., "High-order accurate, low numerical diffusion methods for aerodynamics," *Progress in Aerospace Sciences*, vol. 41, Apr. 2005, pp. 192–300.

[23] Wang, Z. J., "High-order methods for the Euler and Navier–Stokes equations on unstructured grids," *Progress in Aerospace Sciences*, vol. 43, Jan. 2007, pp. 1–41.

[24] Shu, C.-W., "High Order Weighted Essentially Nonoscillatory Schemes for Convection Dominated Problems," *SIAM Review*, vol. 51, Feb. 2009, pp. 82–126.

[25] Chu, P. C., and Fan, C., "A Three-Point Combined Compact Difference Scheme," *Journal of Computational Physics*, vol. 140, Mar. 1998, pp. 370–399.

[26] Bhumkar, Y. G., Sheu, T. W. H., and Sengupta, T. K., "A dispersion relation preserving optimized upwind compact difference scheme for high accuracy flow simulations," *Journal of Computational Physics*, vol. 278, Dec. 2014, pp. 378–399.

[27] Cheong, C., and Lee, S., "Grid-Optimized Dispersion-Relation-Preserving Schemes on General Geometries for Computational Aeroacoustics," *Journal of Computational Physics*, vol. 174, Nov. 2001, pp. 248–276.

[28] Rajpoot, M. K., Sengupta, T. K., and Dutt, P. K., "Optimal time advancing dispersion relation preserving schemes," *Journal of Computational Physics*, vol. 229, May 2010, pp. 3623–3651.

[29] Sengupta, T. K., Lakshmanan, V., and Vijay, V. V. S. N., "A new combined stable and dispersion relation preserving compact scheme for non-periodic problems," *Journal of Computational Physics*, vol. 228, May 2009, pp. 3048–3071.

[30] Tam, C. K. W., and Webb, J. C., "Dispersion-Relation-Preserving Finite Difference Schemes for Computational Acoustics," *Journal of Computational Physics*, vol. 107, Aug. 1993, pp. 262–281.

[31] Cunha, G., and Redonnet, S., "On the effective accuracy of spectral-like optimized finite-difference schemes for computational aeroacoustics," *Journal of Computational Physics*, vol. 263, Apr. 2014, pp. 222–232.

[32] Liu, Y., Vinokur, M., and Wang, Z. J., "Spectral difference method for unstructured grids I: Basic formulation," *Journal of Computational Physics*, vol. 216, Aug. 2006, pp. 780–801.

[33] Wang, Z. J., Liu, Y., May, G., and Jameson, A., "Spectral Difference Method for Unstructured Grids II: Extension to the Euler Equations," *Journal of Scientific Computing*, vol. 32, Jun. 2007, pp. 45–71.

[34] Balan, A., May, G., and Schöberl, J., "A stable high-order Spectral Difference method for hyperbolic conservation laws on triangular elements," *Journal of Computational Physics*, vol. 231, Mar. 2012, pp. 2359–2375.

[35] Wang, Z. J., "Spectral (Finite) Volume Method for Conservation Laws on Unstructured Grids: Basic Formulation," *Journal of Computational Physics*, vol. 178, May 2002, pp. 210–251.

[36] Liu, Y., Vinokur, M., and Wang, Z. J., "Spectral (finite) volume method for conservation laws on unstructured grids V: Extension to three-dimensional systems," *Journal of Computational Physics*, vol. 212, Mar. 2006, pp. 454–472.

[37] Sun, Y., Wang, Z. J., and Liu, Y., "Spectral (finite) volume method for conservation laws on unstructured grids VI: Extension to viscous flow," *Journal of Computational Physics*, vol. 215, Jun. 2006, pp. 41–58.

[38] Wang, Z. J., and Liu, Y., "Extension of the spectral volume method to high-order boundary representation," *Journal of Computational Physics*, vol. 211, Jan. 2006, pp. 154–178.

[39] Qiu, J., and Shu, C.-W., "Hermite WENO schemes and their application as limiters for Runge–Kutta discontinuous Galerkin method: one-dimensional case," *Journal of Computational Physics*, vol. 193, Jan. 2004, pp. 115–135.

[40] Qiu, J., and Shu, C.-W., "Hermite WENO schemes and their application as limiters for Runge–Kutta discontinuous Galerkin method II: Two dimensional case," *Computers & Fluids*, vol. 34, Jul. 2005, pp. 642–663.

[41] Zhu, J., and Qiu, J., "Hermite WENO Schemes and Their Application as Limiters for Runge-Kutta Discontinuous Galerkin Method, III: Unstructured Meshes," *Journal of Scientific Computing*, vol. 39, May 2009, pp. 293–321.

[42] Balsara, D. S., Altmann, C., Munz, C.-D., and Dumbser, M., "A sub-cell based indicator for troubled zones in RKDG schemes and a novel class of hybrid RKDG+HWENO schemes," *Journal of Computational Physics*, vol. 226, Sep. 2007, pp. 586–620.

[43] Luo, H., Baum, J. D., and Löhner, R., "A Hermite WENO-based limiter for discontinuous Galerkin method on unstructured grids," *Journal of Computational Physics*, vol. 225, Jul. 2007, pp. 686–713.

[44] Luo, H., Xia, Y., Li, S., Nourgaliev, R., and Cai, C., "A Hermite WENO reconstruction-based discontinuous Galerkin method for the Euler equations on tetrahedral grids," *Journal of Computational Physics*, vol. 231, Jun. 2012, pp. 5489–5503.

[45] Luo, H., Xia, Y., Spiegel, S., Nourgaliev, R., and Jiang, Z., "A reconstructed discontinuous Galerkin method based on a Hierarchical WENO reconstruction for compressible flows on tetrahedral grids," *Journal of Computational Physics*, vol. 236, 2013, pp. 477–492.

[46] Liu, X., Zhang, S., Zhang, H., and Shu, C.-W., "A new class of central compact schemes with spectral-like resolution I: Linear schemes," *Journal of Computational Physics*, vol. 248, Sep. 2013, pp. 235–256.

[47] Liu, X., Zhang, S., Zhang, H., and Shu, C. W., "A new class of central compact schemes with spectral-like resolution II: Hybrid weighted nonlinear schemes," *Journal of Computational Physics*, vol. 284, Mar. 2015, pp. 133–154.

[48] Wang, Z., Li, J., Wang, B., Xu, Y., and Chen, X., "A new central compact finite difference scheme with high spectral resolution for acoustic wave equation," *Journal of Computational Physics*, vol. 366, 2018, pp. 191–206.

[49] Tao, Z., Li, F., and Qiu, J., "High-order central Hermite WENO schemes: Dimension-by-dimension moment-based reconstructions," *Journal of Computational Physics*, vol. 318, 2016, pp. 222–251.

[50] Zhong, X., "High-Order Finite-Difference Schemes for Numerical Simulation of Hypersonic Boundary-Layer Transition," *Journal of Computational Physics*, vol. 144, Aug. 1998, pp. 662–709.